



# Synthesis and biological evaluation of a ring analogs of the selective CB2 inverse agonist SMM-189

Sahar S. Alghamdi, Suni M. Mustafa, Bob M. Moore II \*

Department of Pharmaceutical Sciences, College of Pharmacy, University of Tennessee Health Science Center, Memphis, TN 38163, USA

## ARTICLE INFO

### Keywords:

Cannabinoids  
Inverse agonist  
CB2 receptor  
cAMP  
 $\beta$ -Arrestin  
Microglia  
Polarization

## ABSTRACT

Microglia are the principle cell type driving sustained neuroinflammation in neurodegenerative diseases such as Alzheimer's, Parkinson's, and Multiple Sclerosis. Interestingly, microglia locked into a chronic M1 pro-inflammatory phenotype significantly up-regulate the cannabinoid receptor 2 (CB2) expression. Our approach to exploiting CB2 as a therapeutic target in neuroinflammatory diseases focuses on the development of selective CB2 inverse agonists to shift microglia bias to a M2 pro-wound healing phenotype. Herein we report work designed to refine the structure activity relationship of the 2,6-dihydroxy-biphenyl-aryl-methanone CB2 inverse agonist scaffold. A series of analogs of our lead compound SMM-189 were synthesized and measured for affinity/selectivity, potency, and efficacy in regulating cAMP production and  $\beta$ -arrestin recruitment. In this series compound **40** demonstrated a significant increase in potency and efficacy for cAMP stimulation compared to SMM-189. Akin to our lead SMM-189, this compound was highly efficacious in biasing microglia to an M2 pro-wound healing phenotype in LPS stimulated cell lines. These results advance our understanding of the structure-activity relationship of the 2,6-dihydroxy-biphenyl-aryl-methanone scaffold and provide further support for regulating microglia activation using CB2 inverse agonists.

## 1. Introduction

Inflammation and dysregulated immune responses are an underlying pathology in a broad range of diseases such as inflammatory bowel disease,<sup>1</sup> cancer,<sup>2</sup> and neurodegenerative disorders.<sup>3</sup> Non-steroidal anti-inflammatory drugs and glucocorticoids are the mainstays for acute inflammation; however, side effects from long-term NSAIDs therapy, e.g. gastrointestinal tract side-effects,<sup>4</sup> or glucocorticoid-induced osteoporosis<sup>5</sup> can complicate their use in chronic inflammatory diseases. Disease-modifying drugs, such as methotrexate and leflunomide, are effective in treating autoimmune diseases but can exhibit reduced efficacy over time.<sup>6</sup> More recently biologicals, e.g. Infliximab and Humira, have had a significant impact in regulating several peripherally mediated inflammatory/immune responses in diseases including rheumatoid arthritis, psoriasis, and, Crohn's disease.<sup>7</sup> Most of these approaches however have limited efficacy in the treatment of inflammation and dysregulated immune responses in the central nervous system (CNS). The limited efficacy is in large part caused by the blood-brain barrier (BBB) that excludes approximately 98 percent of small molecule drugs and all of the high molecular weight biologicals.<sup>8</sup> Although the integrity

of the BBB declines in many neurodegenerative disorders, repurposing existing anti-inflammatory and/or immune regulatory drugs has proven challenging.<sup>9</sup> Unfortunately, neuroinflammation is an underlying pathology in CNS diseases, such as traumatic brain injury,<sup>10</sup> Alzheimer's<sup>11</sup> and Parkinson's diseases<sup>12</sup>, which contributes to disease progression. As such, there remains a critical unmet need for new therapeutic approaches to regulate neuroinflammation.

Acute neuroinflammation plays a key role in resolving and healing damage to the brain; however, the progression into chronic inflammation ultimately exacerbates the initial injury. The principal mediator of neuroinflammation are microglia,<sup>13</sup> the CNS equivalent of the macrophage, which is the central target of many anti-inflammatory strategies. For example, in neurodegenerative disorders, several existing drugs, such as thalidomide,<sup>14</sup> minocycline,<sup>15</sup> psychiatric drugs,<sup>16</sup> and thiazolidinediones<sup>17</sup> have been investigated as potential regulators of microglial activation. *In vitro*, these compounds are effective in reducing the pro-inflammatory M1 microglia activation state and, in some cases, promoting the pro-wound healing M2 state. However, the efficacy in halting neuroinflammation of Alzheimer's, Parkinson's, and traumatic brain injury remains controversial. More recently the cannabinoid

\* Corresponding author at: 881 Madison Ave., Room 563, Memphis, TN 38163, USA.

E-mail address: [bmoore@uthsc.edu](mailto:bmoore@uthsc.edu) (B.M. Moore II).

<https://doi.org/10.1016/j.bmc.2021.116035>

Received 17 December 2020; Received in revised form 14 January 2021; Accepted 16 January 2021

Available online 25 January 2021

0968-0896/© 2021 Elsevier Ltd. All rights reserved.

receptor 2 (CB2) has emerged as an important target for the development of therapeutics to treat microglia-mediated neuroinflammation.<sup>18</sup> Interestingly, in the resting state, microglia express low levels of CB2 but the expression is significantly up-regulated in response to CNS insult. Evidence indicates that CB2 upregulation is a conserved microglia response to activation. Specifically, CB2 up-regulation on microglia has been found in post-mortem brains of Parkinson's,<sup>19</sup> Alzheimer's,<sup>20</sup> and human immunodeficiency virus encephalitis,<sup>21</sup> and in the spinal cords of multiple sclerosis and amyotrophic lateral sclerosis.<sup>22</sup> Presumably, CB2 is also up-regulated in traumatic brain injury because post-mortem brains of patients also exhibit microglia activation.<sup>23</sup> In sum, the expression of CB2 on activated microglia present a unique target for regulating the progressive CNS damage associated with chronic neuroinflammation.

The CB2 receptor is a constitutively active G-protein coupled receptor that couples to G<sub>αi</sub>.<sup>24–26</sup> The receptor is widely distributed in the peripheral immune cells making it an important target for regulating inflammation and immune activity.<sup>27,28</sup> Selective agonists of CB2 are by far the most structurally diverse and mature class of ligands representing at least 12 candidates that have entered into clinical trials (reviewed by Dhopeswarkar and Mackie<sup>29</sup> and Tabrizi and colleagues<sup>30</sup>). However, the constitutive activity of CB2 also allows for the design of inverse agonists providing an alternate mechanism to regulate CB2 function.<sup>31,32</sup> This class of CB2 selective ligands, which includes SR144528, Sch.336, and JTE-907 (Fig. 1), have been reported to regulate immune cell function and/or inflammation.<sup>33–35</sup> We have also developed a selective CB2 inverse agonist based on the 2,6-dihydroxy-biphenyl-aryl-methanone scaffold. Our lead compound, SMM-189 (Fig. 1) is a potent *in vitro* inhibitor of microglia polarization to the M1 pro-inflammatory phenotype while promoting an M2 pro-healing phenotype.<sup>36</sup> The compound also inhibits the expression of pro-inflammatory cytokines and chemokines in primary human and murine microglia.<sup>36,37</sup> *In vivo*, SMM-189 alleviated or reduced the adverse physiological and psychological effect of mild traumatic brain injury in mice.<sup>37–40</sup> Recently, we reported the administration of SMM-189 in the kainate-induced mouse status epilepticus model protected against neuronal damage and reduced inflammatory markers.<sup>41</sup> The promising *in vivo* activity of SMM-189 demonstrates the potential of the 2,6-dihydroxy-biphenyl-aryl-methanone scaffold for developing novel CB2 inverse agonists. Therefore, to

refine the structure–activity relationship of the scaffold, a series of A ring-substituted analogs of SMM-189 were synthesized. Analog biological activity was measured in CB1 and CB2 binding assays, functional activity in the ACTOne cAMP assay, and inhibition of β-arrestin recruitment in the Tango-BLA. Finally, LPS stimulated murine and human microglial cell lines were assayed for M1 versus M2 bias following treatment with compound 40, the most potent compound in the series.

## 2. Results and discussion

### 2.1. Chemistry

Our first series of 2,6-dihydroxy-biphenyl-aryl-methanone CB2 inverse agonists were designed to test the effects of C ring substituents on biological activity.<sup>42</sup> Out of the 21 compounds in the series, the 4-ethylphenyl and 4-propylphenyl C ring analogs were measured to have increased affinity, potency, and efficacy at CB2 relative to SMM-189. Additionally, the resorcinol hydroxyl groups were discovered to be essential since methylation of one or both hydroxyl groups abolished activity. Within this series the 3,5-dichlorophenyl A ring of SMM-189 was preserved, which left open the question of the effects of A ring substitution on CB1/CB2 receptor activity. To refine the SAR of this structural class of CB2 inverse agonists, the second series of A ring-substituted analogs were synthesized. The C ring substitution in this series was phenyl or thiophenyl, the latter of which demonstrated efficacy in our selective CB2 agonist.<sup>43</sup>

The 2,6-dihydroxy-biphenyl-aryl-methanone compounds were previously synthesized starting from syringaldehyde; however, removal of the methyl protecting groups required heating to 220 °C in pyridine hydrochloride.<sup>42</sup> While successful, to obtain products of 96 percent or greater purity for biological testing, some of the final products required re-crystallization and/or preparative HPLC purification. To circumvent the challenging deprotection, the methoxymethyl (MOM) group was selected due to milder deprotection conditions. Syringaldehyde was unsuitable as a starting material since 4 steps would be required to exchange the methyl groups for MOM. Additionally, the Suzuki–Miyaura cross-coupling was carried out using the pseudohalide triflate ester. The formation of the ester required triflic anhydride which we sought to

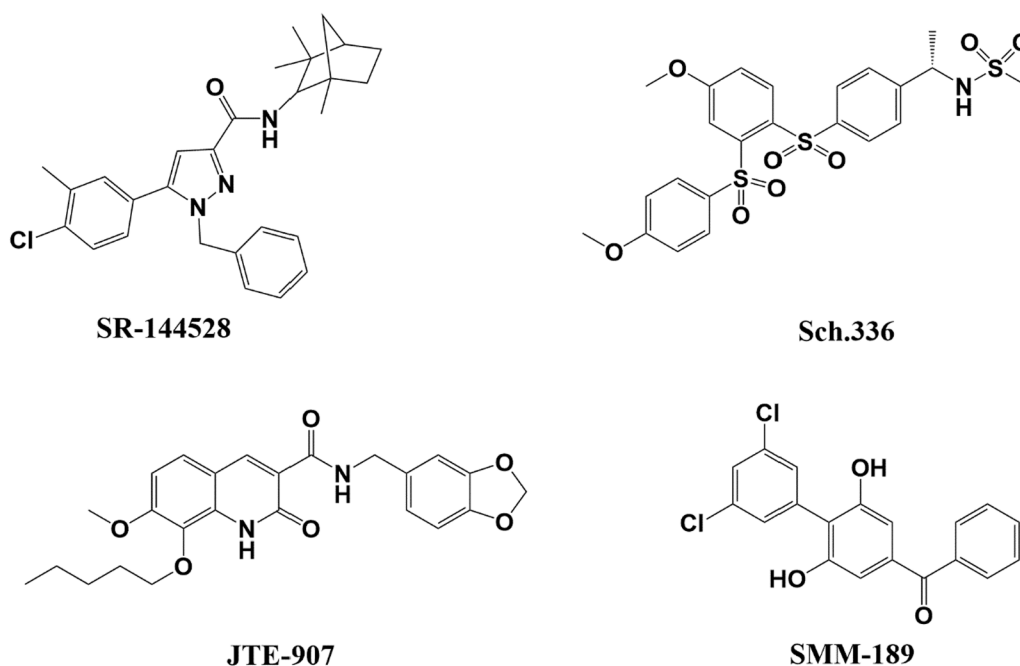


Fig. 1. Selective CB2 inverse agonists.

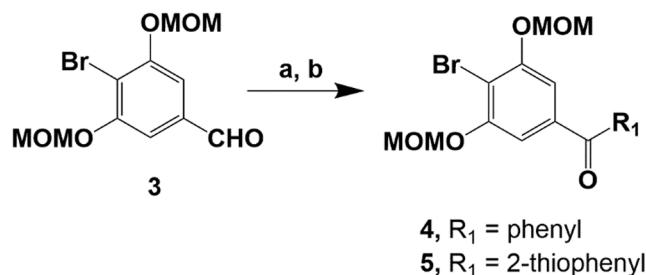
eliminate to reduce synthetic cost. Based on the functional group requirements to conduct the transformation necessary to prepare the target compounds intermediate **3** was identified.

Synthesis of intermediate **3** was accomplished in 4 steps beginning with the regioselective 4-bromination 3,5-dihydroxybenzoic acid (**1**) according to the method of Fillion and Fishlock.<sup>44</sup> Introduction of the MOM groups was carried out using *in situ* generated MOMCl as reported by Berliner and Belecki.<sup>45</sup> This approach limited exposure to the MOMCl, which is toxic and carcinogenic, and provided a highly reactive reagent compared to some commercial sources. Reduction of the MOM ester with DIBAL and subsequent oxidation using PCC provided intermediate **3** in 61% overall yield (Scheme 1). The C ring was introduced in 2 steps via a reaction of **3** with either phenyl magnesium bromide or 2-thiophenyl magnesium bromide followed by PCC oxidation to yield intermediate ketones **4** and **5** (Scheme 2). Introduction of the A ring was accomplished via a Suzuki–Miyaura cross-coupling using Buchwald precatalysts Pd-G3 SPhos in a THF-0.5 N potassium triphosphate solvent system (Scheme 3). Deprotection using 3 N hydrochloric acid in ethanol yielded the target resorcinol products.

## 2.2. Receptor binding

The binding affinities of compounds **20–33** and **40–45** for the hCB1 and hCB2 receptors were measured in competition radioligand displacement assays using membrane preparations from the ACTOne cell lines and [<sup>3</sup>H] CP 55,940.<sup>42</sup> Our lead compound SMM-189 contained a 3,5-dichlorophenyl A ring suggesting electronegative groups are favored. However, the substitution of this group with 3,5-difluorophenyl (**21**) surprisingly reduced hCB2 affinity by an order of magnitude (121.3 nM versus 1,634 nM) and increased hCB1 affinity from 4.78 μM to 1.08 μM with a hCB1/hCB2 selectivity ratio (SR) of 0.66 compared to 39.4 for SMM-189 (Table 1). The decrease in the affinity of **21** may reflect a reduction in the size of the electronegative group which is supported by compound **23** which contains the 3,5-bis-(trifluoromethyl) phenyl group. Specifically, this A ring substitution restored hCB2 affinity ( $K_i = 215$  nM) but negatively affected selectivity (SR = 8.86) due to increased binding to hCB1 ( $K_i = 1.90$  μM). Removal of the trifluoromethyl group in the 5 positions (**20**) eliminated binding to CB1 while retaining affinity for hCB2 ( $K_i = 204$  nM) increasing the SR to 49. Substitution of the 3-trifluoromethyl with 3-methyl (**24**) modestly decrease hCB2 affinity ( $K_i = 320$  nM) with a concomitant increase for hCB1 ( $K_i = 4.01$  μM). Interestingly, the 2,5-dichlorophenyl (**22**) caused a slight decrease in hCB2 binding ( $K_i = 233$  nM) but increased SR to 42.9 by inhibiting hCB1 binding. The A ring in **22** can be alternatively numbered 3,6-dichlorophenyl suggesting that electronegative groups in the 3 position of the A ring are important for receptor selectivity.

We previously reported that SMM-189 exhibits orthosteric binding to hCB2 in competition functional assays against CP-55,940.<sup>42</sup> This determination, in combination with the presence of a methylenehydroxy group in HU-210, suggested that an A ring containing a 3-hydroxymethylene (**27**) group would enhance affinity for hCB2. Surprisingly, compound **27** had a poor affinity for hCB2 ( $K_i = 2.49$  μM) and did not displace CP 55,940 at CB1. Larger functional groups on the A ring and substitution of the 4 positions were equally detrimental to hCB2 binding as demonstrated by the poor affinity (1.84 to 4.74 μM) of the 4-fluoro-3-



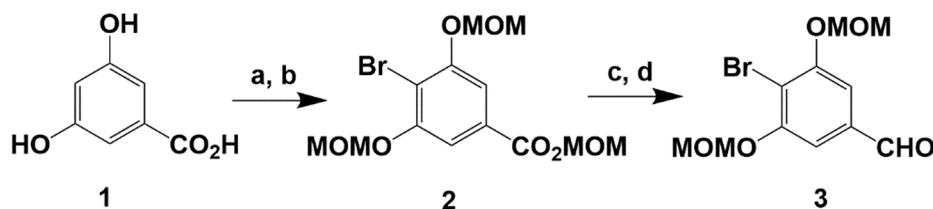
**Scheme 2.** Reagents and conditions: (a) phenyl- or thienyl-magnesium bromide, THF, 0 °C → r.t.; (b) PCC, DCM, r.t.

cyano (**28**), 3,4-methylenedioxy (**25**), and 2,3-dihydro-benzo[1,4] dioxin (**26**) analogs for hCB2. These results suggest that in the ligand-binding pocket the A ring occupies a sterically limited site. Replacement of the phenyl A ring with a pyridyl ring (**29**) was equally ineffective. The addition of electronegative groups to the pyridyl ring, *i.e.* fluorine (**30**) and chlorine (**31**), in the 3-position relative to compounds **20** and **22**, abolished binding to both hCB1 and hCB2. It is presumed that the pyridyl group would be protonated under the assay conditions suggesting unfavorable charge-charge interactions in the ligand-binding pocket of both receptors. Interestingly replacement of the A ring with the neutral, ring contracted heterocycles furanyl (**33**) and thiophenyl (**32**) shifted receptor activity. In the case of **33** ( $K_i = 1.33$  μM) the functional activity in the cAMP assay switched from an inverse agonist to a partial agonist. The thiophenyl substitution (**33**) abolished binding to hCB1 and hCB2. The results for the 5 membered heterocycles suggest that compound **33** binds in a different orientation to hCB2 relative to the phenyl ring analogs.

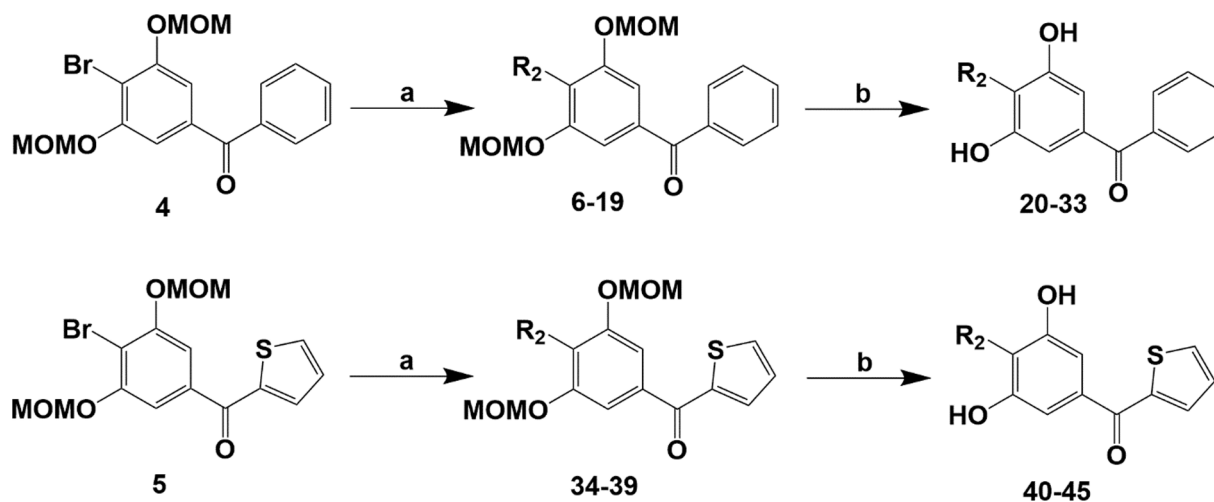
The results from our earlier work on C1' substituted classical cannabinoids<sup>46</sup> and biaryl-aryl hCB2 agonist<sup>43</sup> revealed that a thiophene ring increased hCB2 affinity. To determine if this transformation could improve inverse agonist activity compounds **40–45** were synthesized wherein the phenyl C ring was replaced by thiophenyl. In the case of the 3-trifluoromethyl (**40**) and 3,5-trifluoromethyl (**42**) analogs, the thiophenyl group increased binding to 154 and 187 nM, respectively, with SRs of 64.9 and 20 (Table 2). However, this transformation resulted in a 3-fold decrease in hCB2 affinity in the 3-methylphenyl (**41**) analog ( $K_i = 975$  nM) compared to the phenyl C analog (**24**) affinity of 320 nM and a 2 fold decrease in hCB1 binding (4.02 μM versus 9.53 μM). In a similar trend, the thiophenyl C ring decreased the affinity of the 2,5-dichlorophenyl (**43**) 2-fold, the 3-hydroxymethylene phenyl (**44**) 3-fold, and abolished binding in the 3-pyridyl analog (**45**). Overall, replacement of the 3,5-dichlorophenyl A ring in SMM-189 with different functional groups did not improve hCB2 affinity; however, the 3-trifluoromethyl group did abolish hCB1 affinity providing SRs of 49 and 65 for compounds **20** and **40**, respectively, compared to 39.4 for SMM-189.

## 2.3. Functional assays

The ACTOne functional assay was used to measure the potency and efficacy of compounds **20–33** and **40–45** in regulating cAMP production in cells expressing either hCB1 or hCB2 or the parental line containing



**Scheme 1.** Reagents and conditions: (a) 20% HCl, Br<sub>2</sub>, Δ; (b) i. dimethoxymethane, acetylchloride, zinc bromide, 0 °C, ii. DCM, 4-bromo-3,5-dihydroxybenzoic acid, iii. DIEA, 0 °C → r.t.; (c) DIBAL, THF, 0 °C → r.t.; (d) PCC, DCM, r.t.



Scheme 3. Reagents and conditions: (a) aryl/heteroaryl boronic acid, Pd-G3 SPhos, THF, 0.5 N  $K_3PO_4$ , r.t.; (b) 3 N HCl in ethanol.

only the cAMP gated ion channel. The reference compound CP-55,940 was a potent agonist at hCB1 ( $pEC_{50} = 8.70$ ) and hCB2 ( $pEC_{50} = 8.20$ ) with cAMP suppression efficacies of  $-94.6$  and  $-77.8$ , respectively (Table 4). In the hCB1 assay, none of the compounds were active (Tables 3 and 4) nor was there response in the parental cell line indicating no off-target effects. A linear regression of  $\log(1/K_i)$  versus  $\log(1/EC_{50})$  for compounds active in the hCB2 cAMP assay yielded an  $R^2 = 0.56$  wherein the compounds outside the 95% confidence interval were the thiophenyl analogs 40–43 and compound 24 (Fig. 2). There are insufficient compounds in the thiophenyl series to determine if separate correlations can be established between the series. Notwithstanding, the thiophenyl C ring (compounds 40, 41, and 43) improves potency compared to the phenyl C ring analogs (compounds 20, 22, and 24) for the 3-trifluoromethyl- ( $pEC_{50}$  7.41 versus 6.62), 3-methyl- ( $pEC_{50}$  6.70 versus 5.78), and the 2,5-dichloro- ( $pEC_{50}$  6.85 versus 6.44) functional groups. Within this group of compounds, only compound 40 had a statistically significant increase in potency with  $p$  values ranging from 0.05 to 0.0001. In terms of efficacy (% max), none of the compounds significantly increased cAMP levels above the lead compound SMM-189 and a significant decrease was measured for compound 24 ( $p = 0.05$  to 0.001). The conversion of the C ring phenyl to thiophenyl in the 3,5-trifluoromethyl analogs, 23 and 42 respectively, did not significantly affect potency but did significantly increase efficacy ( $p = 0.0001$ ) in the thiophenyl analog. Although the replacement of the 3,5-dichlorophenyl ring in SMM-189 with 3,5-difluorophenyl (21) negatively affected affinity and potency, the efficacy was not significantly different from potent and efficacious compounds such as 40. Surprisingly, compound 33, wherein the A ring is 3-furanyl, was measured to have weak agonist activity with a  $pEC_{50}$  of 5.56 and efficacy of  $-18.5$ .

Based on receptor theory, inverse agonists do not bind to an active conformation of a constitutively active G-protein coupled receptor, nor do they cause a conformational change leading to an active conformation. In turn, recruitment of  $\beta$ -arrestin would not be predicted since the C-terminus would not be accessible for phosphorylation by G-protein receptor kinases. To measure  $\beta$ -arrestin recruitment we selected the Tango-BLA  $\beta$ -arrestin functional assay which has been reported to provide reliable  $EC_{50}$ s for cannabinoid receptor inverse agonists.<sup>47</sup> Treatment of cells expressing either hCB1 or hCB2 with the non-selective agonist CP-55,940 resulted in cleavage of the CCF4/AM fluorogenic reporter substrate. The  $pEC_{50}$  in the hCB1 assay was 8.24 and 7.43 in the hCB2 assay with efficacies of 4.51 and 3.70, respectively (Table 5). To measure the efficacy of our inverse agonist in this assay, we selected compounds SMM-189, 20–24, 28, and 40–43 based on affinity and potency in ACTOne functional assay. Dose-response studies revealed that none of the nine compounds, or the selective CB2 inverse agonist

SR-144528, activated  $\beta$ -arrestin recruitment in either hCB1 or hCB2 assays. The absence of activity at hCB2 was consistent with inverse agonist activity wherein the ligands bind to inactive receptor conformations. Based on these results we conducted competition assays in the presence of CP-55,940 at an  $EC_{80}$  concentration in the hCB2 cell line. The  $pEC_{50}$  of CP-55,940 was significantly reduced in the presence of SMM-189, analogs 20–24, 40–43, and SR-144528 with values tightly clustered from 5 to 5.9. Compound 28 failed to inhibit  $\beta$ -arrestin recruitment presumably due to low affinity and efficacy, as measured in the ACTOne assay. A linear regression of  $\log(1/K_i)$  versus  $\log(1/Efficacy)$  exhibits good correlation with an  $R^2 = 0.72$  which is consistent with higher affinity compounds displacing a greater fraction of the CP-55,940. In sum, the results from the binding, cAMP, and  $\beta$ -arrestin functional assays establish the SMM-189 analogs as selective inverse agonists at hCB2.

#### 2.4. Effects of compound 40 on LPS activated microglia polarization

The impetus behind the continued refinement of the structure–activity relationship of the 2,6-dihydroxy-biphenyl-aryl-methanone scaffold is the remarkable activity of CB2 inverse agonists, e.g. SMM-189 and SR-144528, to bias activated microglia to a pro-healing M2 phenotype.<sup>36</sup> To continue validating therapeutic potential CB2 inverse agonists, compound 40 was selected to measure the effects on LPS activated murine and human microglia. Compound 40 was first tested for M1/M2 phenotype bias using the C8B4 microglia cell line, which is reported to express the closest features to the native mouse microglia.<sup>48</sup> To assess M1/2 surface markers, C8B4 cells were stimulated with LPS (1  $\mu$ g/ml) for 1 h. The cells were then treated with 20  $\mu$ M compound 40, based on the  $EC_{50}$  in cytotoxicity assays, and incubated for 24 h. The effects on the M1 pro-inflammatory (CD 16/32 and CD 68) and M2 anti-inflammatory (CD 204 and CD 206) markers were evaluated using the on-cell polarization assay previously developed in our lab.<sup>36</sup> Consistent with our previous findings with SMM-189, compound 40 significantly suppressed the M1 associated markers CD 16/32 ( $p < 0.01$ ) and CD 68 ( $p < 0.001$ ) relative to LPS (Fig. 3). Moreover, treatment significantly enhanced the expression of M2 markers CD 204 and CD 206 in comparison to LPS ( $P < 0.0001$ ). To determine if inter-species differences in microglial responses to CB2 inverse agonist could change the M1/M2 phenotype bias, the polarization studies were repeated in SV40 immortalized human microglia. In this study, cells were activated with LPS (100 ng/ml) for 1 h followed by treatment with 40 (35  $\mu$ M) at the previously determined cytotoxic  $EC_{50}$ . Rewardingly, the expression of M1 markers CD 16 ( $p < 0.001$ ) and CD 68 ( $p < 0.0001$ ) were decreased relative to LPS control (Fig. 4). Additionally, the expression of M2

**Table 1**  
Binding affinities of compounds 20–33 for the hCB1 and hCB2 receptors.

Compound	R <sub>2</sub>	CB1 K <sub>i</sub> (nM)	CB2 K <sub>i</sub> (nM)	CB1:CB2 ratio
20		>10,000	204 ± 40.6	49.0
21		1,076 ± 91.4	1,634 ± 45.8	0.66
22		>10,000	233 ± 45.5	42.9
23		1,904 ± 77.7	215 ± 54.4	8.86
24		4,015 ± 142.9	320 ± 59.2	12.6
25		>10,000	>10,000	1
26		>10,000	4,740 ± 74.9	2.11
27		>10,000	2,494 ± 117.6	4
28		>10,000	1,839 ± 61.2	5.44
29		>10,000	>10,000	1
30		>10,000	>10,000	1
31		>10,000	>10,000	1
32		>10,000	>10,000	1
33		>10,000	1,328 ± 56.8	7.53
SMM-189		4,778 ± 246	121.3 ± 20.6	39.4

markers CD 204 and CD 206 were significantly enhanced in comparison to LPS ( $P < 0.01$ ). The polarization of murine and human microglia from a pro-inflammatory M1 phenotype to a pro-wound healing M2 phenotype was further validated in microscopy studies using the human microglial cell line.

Migration and changes in morphology are additional measures of the polarization state of microglia. Therefore, to obtain secondary measurements to support M2 polarization, we conducted scratch assays, to

**Table 2**  
Binding affinities of compounds 40–45 for the hCB1 and hCB2 receptors.

Compound	R <sub>2</sub>	CB1 K <sub>i</sub> (nM)	CB2 K <sub>i</sub> (nM)	CB1:CB2 ratio
40		>10,000	154 ± 1.09	64.9
41		9,526 ± 19.2	975 ± 1.18	9.77
42		3,735 ± 2.39	187 ± 1.11	20.0
43		>10,000	447 ± 1.18	22.4
44		>10,000	8,383 ± 50.1	1.19
45		>10,000	>10,000	1

measure motility and histochemical analysis of cell morphology. In the scratch assay, SV40 immortalized human microglia cells were untreated, treated with LPS (100 ng/ml), or a combination of LPS and **40** (100 ng/ml and 10  $\mu$ M, respectively). Following a 24-hour incubation period, cell counting revealed significant migration ( $p = 0.001$ ) of microglia treated with LPS relative to controls (Fig. 5). In contrast, treatment with **40** significantly reduced migration compared to LPS alone ( $p = 0.001$ ) with no significant difference relative to controls. To confirm that the migration of microglia in the LPS treatment group correlated with an M1 phenotype, and not an M2 activation state, histochemical analysis of control, LPS treated, and LPS plus **40** was conducted. Analysis of the LPS treated group revealed enlarged, flat, rounded cell bodies with fewer projections, *i.e.* amoeboid morphology (Fig. 6), which is consistent with an LPS induced M1 phenotype.<sup>49</sup> Conversely, treatment with compound **40** following activation induced a distinct transformation of microglia into a ramified cell morphology with a small cell body and several elongated projections, indicating microglia adopted an M2 wound-healing phenotype.<sup>50</sup> It is worth noting that all the three treatment groups showed similar nucleus distribution confirming that morphological changes are due to alteration in cell size and shape rather than a change in cell number.

The migration and morphology of activated microglia are but one set of markers used in phenotype characterization. Mediators generated or secreted by M1 activated microglia also exhibit phenotype-specific profiles such as increased pro-inflammatory cytokines, nitric oxide, and reactive oxygen species (ROS). Of note, ROS has been implicated as a major contributor to neuronal death in many neurological diseases.<sup>51</sup> Therefore, to measure the efficacy of **40** to modulate ROS production, and provide corroborating support of the M2 activation state, we tested **40** in a ROS assay using the immortalize human microglia. At 50 min post LPS (100 ng/ml) plus **40** (10  $\mu$ M) there was a significant decrease ( $p < 0.01$ ) in ROS generation relative to the LPS alone group (Fig. 7). After a 24-hour incubation period, the addition of **40** following LPS activation significantly ( $p < 0.0001$ ) suppressed ROS expression. Our findings are consistent with the results reported by Ribeiro et al. wherein SR-144528, a CB2 inverse agonist, significantly inhibits ROS production in LPS

**Table 3**  
Functional activities of compounds 20–33 in the hCB1 and hCB2 ACTOne cAMP assay.

Compound	R <sub>2</sub>	Potency	Efficacy	Potency	Efficacy
		(pEC <sub>50</sub> )	(% max.)	(pEC <sub>50</sub> )	(% max.)
		CB1R		CB2R	
20		n.a.	n.a.	6.62 ± 0.05	66.0 ± 3.5 <sup>****</sup>
21		n.a.	n.a.	5.77 ± 0.13	63.0 ± 1.7 <sup>****</sup>
22		n.a.	n.a.	6.44 ± 0.08	66.5 ± 2.9 <sup>****</sup>
23		n.a.	n.a.	6.43 ± 0.07	22.9 ± 2.4 <sup>****</sup>
24		n.a.	n.a.	5.78 ± 1.09	40.3 ± 3.4 <sup>****</sup>
25		n.a.	n.a.	n.a.	n.a.
26		n.a.	n.a.	5.31 ± 0.39	49.0 ± 2.0 <sup>****</sup>
27		n.a.	n.a.	n.a.	n.a.
28		n.a.	n.a.	5.55 ± 0.27	52.3 ± 2.4 <sup>****</sup>
29		n.a.	n.a.	n.a.	n.a.
30		n.a.	n.a.	n.a.	n.a.
31		n.a.	n.a.	n.a.	n.a.
32		n.a.	n.a.	n.a.	n.a.
33		n.a.	n.a.	5.56 ± 0.46	-18.5 ± 0.3 <sup>**</sup>
SMM-189		n.a.	n.a.	6.81 ± 0.09	54.8 ± 3.2 <sup>**</sup>

\*\* p < 0.01 in comparison to parental HEK-CNG.

\*\*\*\* p < 0.0001 in comparison to parental HEK-CNG.

stimulated murine BV-2 and primary rat microglia.<sup>52</sup> The inhibition of ROS production is consistent with the results of the cell surface marker, motility, and morphology studies indicating that **40** biases activated microglia to an M2 pro-wound healing phenotype. In sum, the study findings, combined with our work on SMM-189 and SR144528, reveal the therapeutic potential of CB2 inverse agonists to slow or halt the

**Table 4**  
Functional activities of compounds 40–45 in the hCB1 and hCB2 ACTOne cAMP assay.

Compound	R <sub>2</sub>	Potency	Efficacy	Potency	Efficacy
		(pEC <sub>50</sub> )	(% max.)	(pEC <sub>50</sub> )	(% max.)
		CB1		CB2	
40		n.a.	n.a.	7.41 ± 0.06	57.2 ± 5.3 <sup>****</sup>
41		n.a.	n.a.	6.70 ± 0.14	51.7 ± 2.8 <sup>****</sup>
42		n.a.	n.a.	6.17 ± 0.37	49.7 ± 3.7 <sup>****</sup>
43		n.a.	n.a.	6.85 ± 0.15	61.0 ± 3.4 <sup>****</sup>
44		n.a.	n.a.	n.a.	n.a.
45		n.a.	n.a.	n.a.	n.a.
CP-55,940		8.70 ± 0.11	-94.6 ± 0.11 <sup>***</sup>	8.20 ± 0.06	-77.8 ± 6.5 <sup>****</sup>

\*\*\* p < 0.001 in comparison to parental HEK-CNG.

\*\*\*\* p < 0.0001 in comparison to parental HEK-CNG.

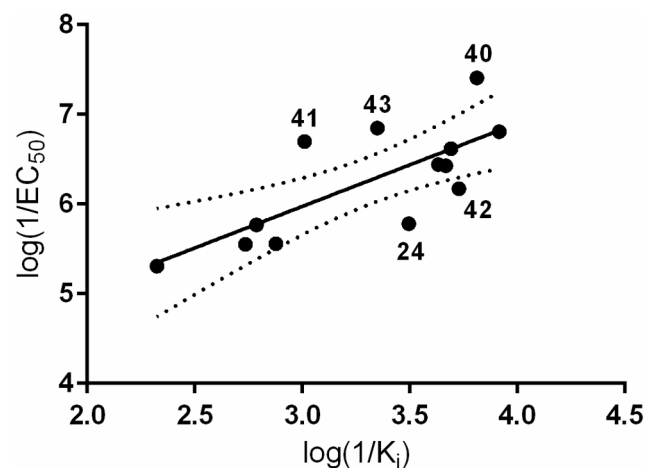


**Fig. 2.** Linear regression of affinity versus potency showing compounds outside the 95% confidence interval (dotted lines).

damaging effects of chronically M1 activated microglia.

### 3. Conclusions

Cannabinoid receptor 2 inverse agonists are a promising new class of therapeutic agents for the treatment of chronic neuroinflammation in debilitating diseases such as Alzheimer's and Parkinson's diseases and traumatic brain injury. We previously identified a new class of CB2 inverse agonists based on the 2,6-dihydroxy-biphenyl-aryl-methanone scaffold, represented by SMM-189, which was highly efficacious in

Table 5

Compound	R <sub>2</sub>	Potency (pEC <sub>50</sub> )	Efficacy (Emission Ratio)	Potency (pEC <sub>50</sub> )	Efficacy (Emission Ratio)
		CB1		CB2	
CP-55,940		8.24 ± 0.27	4.51 ± 0.09	7.43 ± 0.03	3.70 ± 0.06
20		n.a.	n.a.	5.46 ± 0.21	1.41 ± 0.52 ****
21		n.a.	n.a.	5.05 ± 4.27	2.22 ± 0.44 ****
22		n.a.	n.a.	5.22 ± 0.55	1.03 ± 0.20 ****
23		n.a.	n.a.	5.85 ± 0.07	0.91 ± 0.19 ****
24		n.a.	n.a.	<5	2.30 ± 0.12 ****
28		n.a.	n.a.	n.a.	n.a.
SMM-189		n.a.	n.a.	6.81 ± 0.09	0.66 ± 0.08 ****
40		n.a.	n.a.	5.07 ± 0.67	1.19 ± 0.23 ****
41		n.a.	n.a.	5.21 ± 0.81	2.68 ± 0.09 ****
42		n.a.	n.a.	5.89 ± 0.06	0.94 ± 0.09 ****
43		n.a.	n.a.	<5	1.46 ± 0.22 ****
SR-144528		n.a.	n.a.	5.93 ± 0.18	0.65 ± 0.18 ****

\*\*\*\* p < 0.0001 in comparison to CP-55,940.

biasing microglial activation to an M2 phenotype *in vitro* and *in vivo*. To refine the structure–activity relationship of this structural class, a series of twenty SMM-189 analogs were synthesized. The analogs focused on the effects of various A ring functional groups, and C ring thiophenyl substitution, on hCB1/hCB2 affinity/selectivity and potency and efficacy in regulating cAMP production and  $\beta$ -arrestin recruitment. Analysis of the actives of the twenty analogs reveals that substitution of the A ring in the 3-position with electronegative groups approximating the size of chlorine, e.g. trifluoromethyl group in **20** and **40** is optimum for activity. Further improvement in activity was achieved by replacing the C ring

phenyl (**20**) with the 2-thiophenyl functional group (**40**). In general, larger substituents, e.g. **27**, or substitution of the 4-position (**25**) negatively impacted receptor affinity as did replace chlorine with fluorine (**21**). Substitution of the A ring with heterocycles abolished receptor affinity and functional activity. The notable exception was the 2-furanyl in compound **33** that resulted in CB2 partial agonist. Of the compounds synthesized in this series compound, **40** had a significant increase in potency and efficacy for cAMP stimulation relative to SMM-189.

In contrast to the cAMP up-regulation, selected compounds did not stimulate the recruitment of  $\beta$ -arrestin, consistent with binding of an

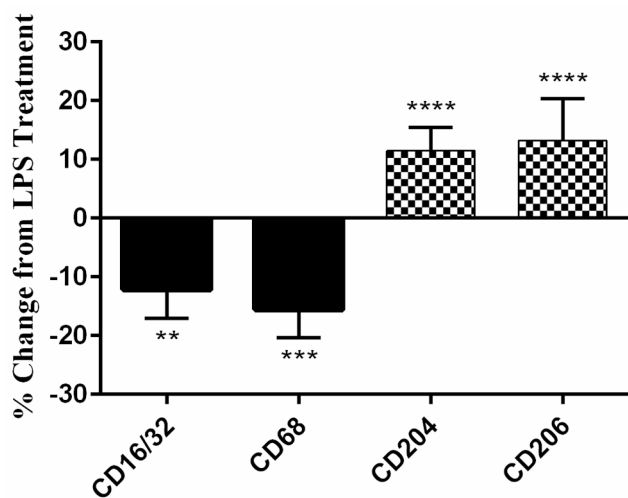


**Fig. 3.** On cell polarizations assays. Treatment of LPS stimulated murine C8B4 microglia with compound **40** caused a significant decrease in M1 markers CD16/32 and CD68 (black bars) 24 h post treatment. In contrast, a significant increase in M2 markers CD204 and CD206 (checkered bars) was measured in the same time interval. Asterisks above columns are comparisons to LPS control with significance designated as \*\*  $P < 0.01$ , \*\*\*  $P < 0.001$ , and \*\*\*\*  $P < 0.0001$ . Data represents 6–9 biological replicates and error is SEM.

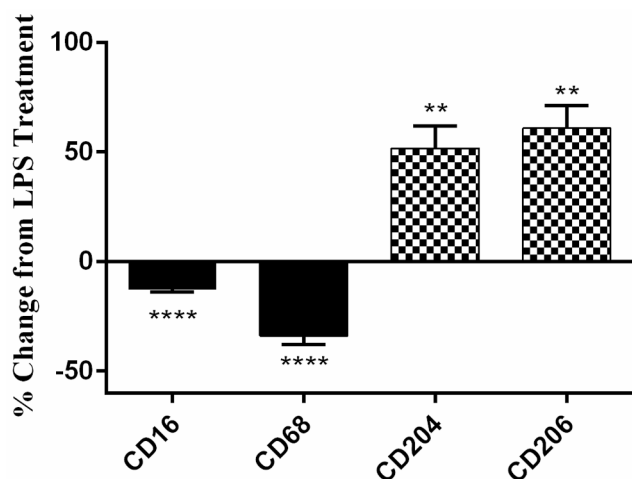


**Fig. 4.** On cell polarizations assays. Treatment of LPS stimulated immortalized human microglia with compound **40** caused a significant decrease in M1 markers CD16 and CD68 (black bars) 24 h post treatment. In contrast, a significant increase in M2 markers CD204 and CD206 (checkered bars) was measured in the same time interval. Asterisks above columns are comparisons to LPS control with significance designated as \*\*  $P < 0.01$  and \*\*\*\*  $P < 0.0001$ . Data represents 6–9 biological replicates and error is SEM.

inverse agonist to an inactive receptor conformation. The SMM-189 analogs did inhibit CP-55,940 stimulated recruitment of  $\beta$ -arrestin, albeit with low  $EC_{50}$ s. This is presumably due to an almost order of magnitude difference in the CB2 affinities of the analogs compared to CP-55,940. To further support our hypothesis that CB2 inverse agonists provide a novel approach to regulating microglia function, the effects of **40** on LPS stimulated microglia were measured. All the phenotypical markers evaluated in this work demonstrate the efficacy of **40** in biasing microglia to a pro-wound healing M2 phenotype. This is evidenced by significant decreases in CD 16/32 and CD 68 (M1 markers), cell migration, and ROS production. Concomitantly, expression of the M2 markers CD 204 and CD 206 significantly increased and a shift from an amoeboid to a ramified (M2 phenotype) morphology was observed. We

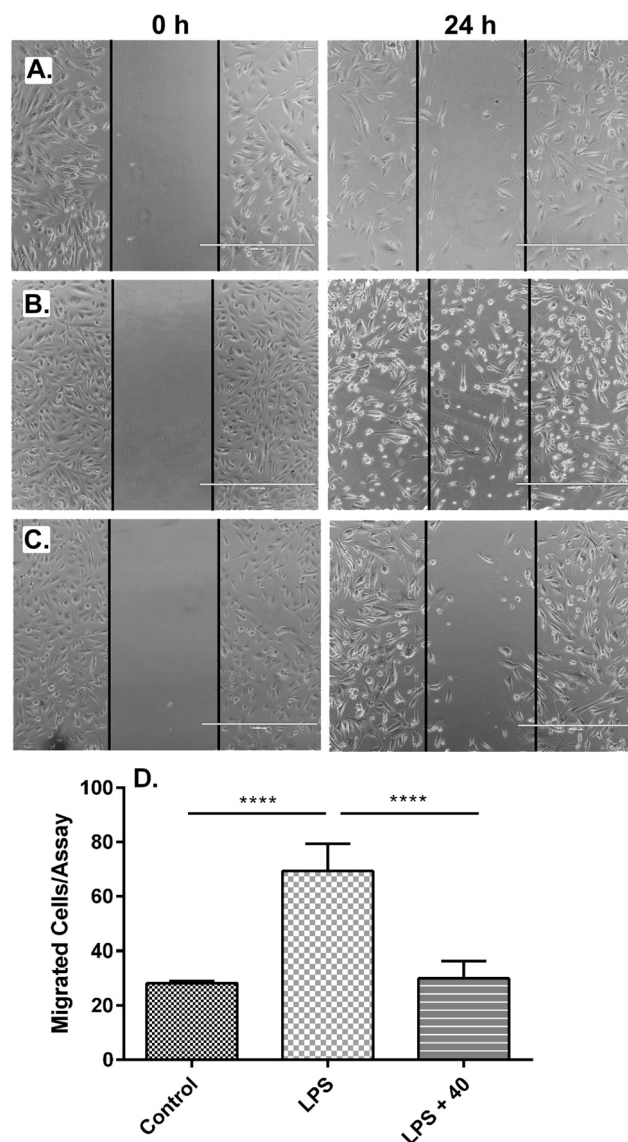


**Fig. 5.** Measurement of immortalized human microglia migration in the scratch assay. Control cells did not exhibit extensive migration 24 h after application of the scratch (Panel A). Stimulation with LPS triggered a significant migration of microglia after 24 h incubation (Panels B and D). Treatment with compounds **40** significantly inhibited LPS stimulated migration to a level which was not significantly different than controls (Panels C and D). Cell migration from 7 biological replicates were measured using ImageJ. Error is reported as SEM, significance is \*\*\*\*  $P < 0.0001$ , the white bar at the bottom of the images represents 1,000  $\mu$ m.

expect that validation of the biological activity in combination with functional activity will guide our development of the structure–activity relationship of the 2,6-dihydroxy-biphenyl-aryl-methanone scaffold leading to a newer more potent CB2 inverse agonist.

## 4. Experimental

### 4.1. Synthesis reagents and supplies

All chemicals and reagents were purchased from Sigma–Aldrich or Fisher Scientific Inc. Anhydrous solvents were prepared by distillation over sodium metal or calcium hydride prior to use. Moisture or oxygen-sensitive reactions were carried out using oven-dried glassware under dry conditions under an argon atmosphere. Analytical thin-layer

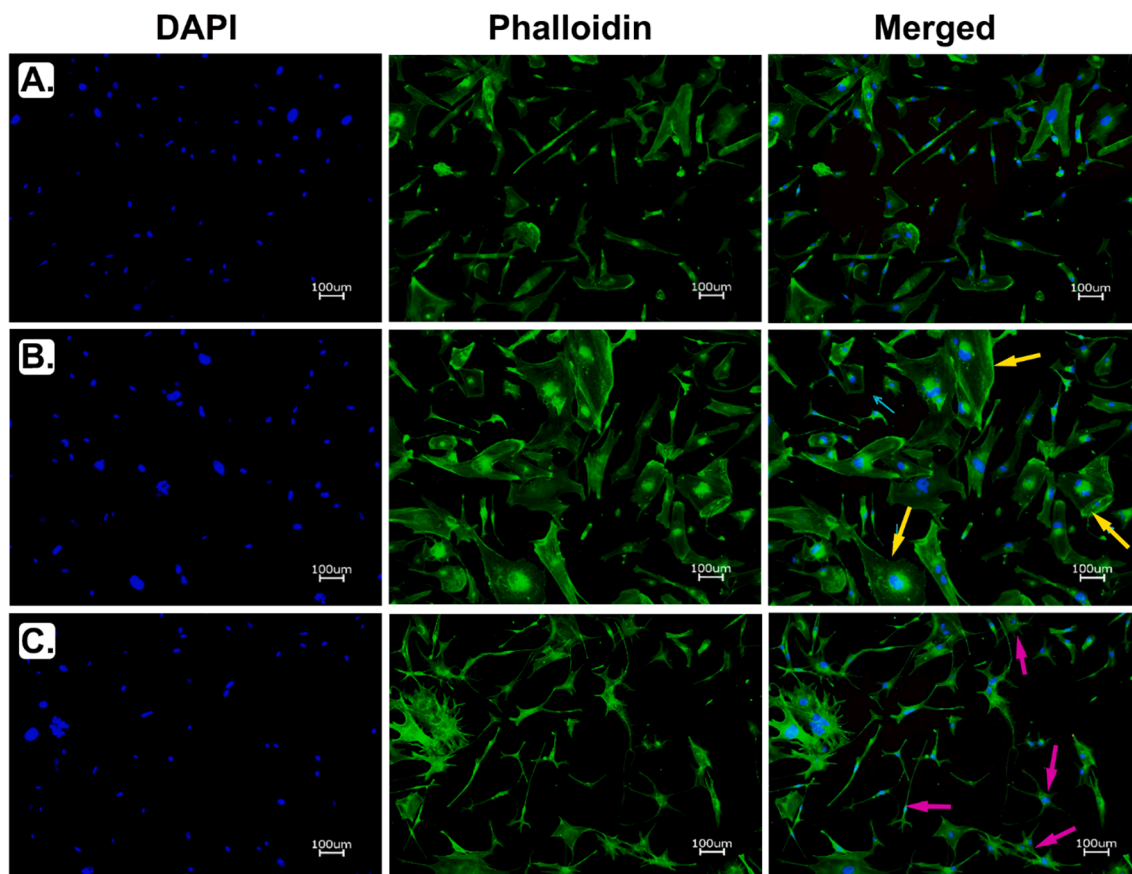


**Fig. 6.** Representative micrographs of immortalized human microglia visualized using DAPI (nuclear stain) and phalloidin F-actin stain. Control cells did not exhibit any morphological changes over the 24 h time course (Panel A). Stimulation with LPS triggered a significant increase in cell size with rounded shape morphology (yellow arrows) after 24 h incubation (Panel B). Treatment with compounds **40** significantly increased the ramified and rod-shaped microglia morphology (magenta arrows) with multiple projections (Panel C). White bars in each photomicrograph represent 100  $\mu\text{m}$  with ten fields collected per group. (For interpretation of the references to colour in this figure legend, the reader is referred to the web version of this article.)

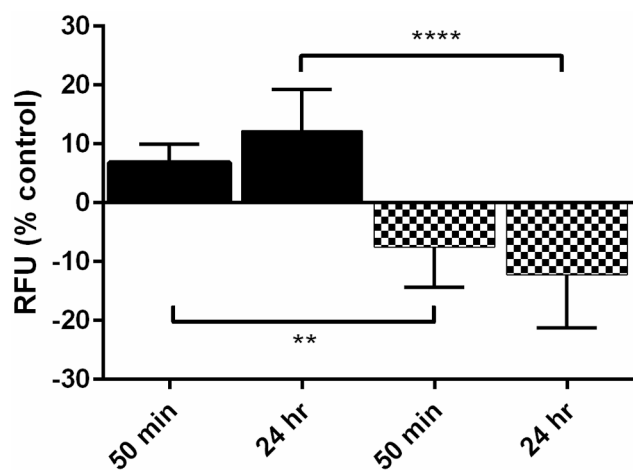


**Fig. 7.** Measurement of immortalized human microglia reactive oxygen species production. Treatment with LPS caused a significant increase in ROS compared to control cells at 50 min and 24 h (black bars). Compound **40** treatment following activation with LPS significantly suppressed ROS generation at both time points compared to LPS alone (checkered bars). Asterisks above columns are comparisons to LPS control with significance designated as \*\*  $P < 0.01$  and \*\*\*\*  $P < 0.0001$ . Data represents 6 biological replicates and error is SEM.

chromatography was performed on Silica G plates Sorbent Technologies (Atlanta, GA) and was visualized by fluorescence quenching under UV light. Compound purification was performed on a Biotage SP1 Flash Chromatography Purification System (Charlotte, NC) using Biotage SNAP Ultra columns. NMR spectra were acquired on a Bruker Ascend 400 (Billerica, MA) spectrometer (400 MHz for  $^1\text{H}$  and 100 MHz for  $^{13}\text{C}$ ). Coupling constants ( $J$ ) are expressed in hertz (Hz) and chemical shifts are reported in ppm on the  $\delta$  scale and referenced to the appropriate solvent peak. Routine mass spectra were collected on a Bruker anaZon SL electrospray/ion trap instrument (Billerica, MA). High-resolution mass spectrometer (HRMS) data and purity were acquired on a Waters Xevo G2 + S QTOF (Milford, MA) system equipped with a Waters Acquity UPLC system. A reversed-phase BEH C18 analytical column (2.1 mm  $\times$  50 mm, 1.7 mm particle size) (Waters, Milford, MA) was used for the LC separation. Acetonitrile and 95% water with 5% acetonitrile were used as the organic (solution B) and aqueous (solution A) mobile phase solutions, respectively. A 5-min gradient elution program was as following: from start – 1.5 min, 20% B; 1.5 min – 3.0 min, 20% to 100% B; 3.0 min–4 min, 100%B; 4–4.5 min 100% to 20% B back to initial condition and finish at 5 min. The total flow rate was at 0.3 mL/min. All target compounds were found to be  $\geq 95\%$  pure by UPLC.

#### 4.2. 4.2 Synthesis

##### 4.2.1. 4-Bromo-3,5-dihydroxybenzoic acid

Into a three-necked 2 L bottom tap flask fitted with a mechanical stirrer and reflux condenser was charged 1 L of 20% HCl, 3,5-dihydroxy benzoic acid (**1**, 100 g, 0.60 mol) and  $\text{Br}_2$  (105 g, 0.65 mol). With

vigorous stirring the suspension was heated to reflux, after 1.5 h the solids dissolved and at 3 h a white solid began to form. The reaction was cooled to room temperature and stirred vigorously overnight. The flask was tapped, and the effluent was directed into a Buchner funnel and the collected solid as air-dried. The light-yellow solid was recrystallized from methanol to yield 127.9 g (91%) of the desired product as a white solid.  $^1\text{H NMR}$ , (400 MHz,  $(\text{CD}_3)_2\text{CO}$ ),  $\delta$  9.16 (br. s, 2H, ArOH), 7.20 (s, 2H, ArH), MS:  $m/z$  (ESI, neg.) = 232.8  $[\text{M}-1]^-$ .

#### 4.2.2. (Methoxy)methyl 3,5-bis(methoxymethoxy)-4-bromobenzoate (2)

Into a 3 L jacketed three neck bottom tap flask equipped with a mechanical stirrer, condenser, and dropping funnel was charged dimethoxymethane (130 g, 151 mL 1.71 mol) and anhydrous zinc bromide (72 mg, 0.32 mmol). The flask was cooled via a circulating ice-cold brine solution. Acetyl chloride (134 g, 121 mL, 1.88 mol) was added to the dropping funnel and an initial aliquot of 6 mL was added followed by drop wise addition of the remaining reagent over 30 min. Two 215 mL aliquots of anhydrous dichloromethane were passed through the funnel and added all at once into the reaction mixture. To the mixture was added 4-bromo-3,5-dihydroxybenzoic acid (107 g, 0.46 mol) and the resulting slurry stirred vigorously. The dropping funnel was charged with *N,N*-diisopropylethylamine (237 g, 317 mL, 1.24 mol) then added dropwise to the mixture over a 1 h period after which cooling was discontinued and the reaction was stirred at room temperature for 12 h. The reaction was quenched with saturated ammonium chloride (200 mL) to which 200 mL of water was then added. The organic phase was collected via the flask tap and the aqueous phase was extracted in the flask with dichloromethane ( $3 \times 200$  mL). The organic fractions were pooled, dried over sodium sulfate, treated with decolorizing carbon, then filtered through a silica/celite column. The volume was reduced to approximately 200 mL under reduced pressure then cooled in an ice bath. The solution was triturated with hexane then the dichloromethane was slowly removed by passing a stream of air over the ice-cold solution. The white crystals were collected by filtration and dried to yield 143.8 g (86%) of **2**.  $^1\text{H NMR}$ , (400 MHz,  $\text{CDCl}_3$ ),  $\delta$  7.52 (s, 2H, ArH), 5.48 (s, 2H,  $\text{CO}_2\text{CH}_2$ ), 5.27 (s, 4H,  $\text{OCH}_2\text{O}$ ), 3.54 (s, 9H,  $\text{OCH}_3$ ), MS:  $m/z$  (ESI, pos.) = 388.9  $[\text{M} + 23]^+$ .

#### 4.2.3. (3,5-bis(methoxymethoxy)-4-bromophenyl) methanol

Into a 5 L bottom tap three necked flask fitted with a mechanical stirrer, dropping funnel, and gas inlet was charged **2** (143 g, 0.39 mol) and 1.65 L anhydrous THF. The reaction apparatus was flushed with  $\text{N}_2$  then DIBAL (890 mL, 1.1 M solution in cyclohexane, 0.98 mol) was cannula transferred to the funnel. The solution was cooled in a brine/ice bath and DIBAL was added dropwise over 1 h. The ice bath was removed, and the reaction allowed to warm to room temperature. After stirring 2 h at room temperature the reaction was quenched, with cooling, using 50 mL methanol followed by a saturated solution of sodium potassium tartrate (550 g in 800 mL water). The mixture was stirred vigorously for 18 h, phases separated, the organic phase dried over sodium sulfate, and the solvent removed under reduced pressure to yield 98.8 g (83%) of the product as a white solid.  $^1\text{H NMR}$ , (400 MHz,  $\text{CDCl}_3$ ),  $\delta$  6.85 (s, 2H, ArH), 5.26 (s, 4H,  $\text{OCH}_2\text{O}$ ), 4.65 (d,  $J = 5.2$  Hz, 2H,  $\text{CH}_2\text{OH}$ ), 3.52 (s, 6H,  $\text{OCH}_3$ ), 1.96 (t, 1H,  $J = 5.6$  Hz,  $\text{CH}_2\text{OH}$ ), MS:  $m/z$  (ESI, pos.) = 330.9  $[\text{M} + 23]^+$ .

#### 4.2.4. 3,5-bis(methoxymethoxy)-4-bromobenzaldehyde (3)

Into a 5 L three necked bottom tapped flask equipped with a mechanical stirrer was charged PCC (153 g, 0.71 mol) and 2 L of dichloromethane. A solution of (3,5-bis(methoxymethoxy)-4-bromophenyl) methanol in 500 mL of dichloromethane was added to the vigorously stirred mixture and allowed to stir for 20 h at room temperature. The top part was cleared, and the mixture was removed. The tap was closed and 1.5 L of dichloromethane and 2 L of 1 N sodium hydroxide were added and the mixture vigorously stirred until all the solids dissolved and the aqueous phase turned green. The organic phase

was taped off, organic phases combined, then the aqueous phase was removed and allowed to stand to collect waste chromium (III) as a green solid. The combined organic fraction was returned to the flask and 2 L of saturated sodium bicarbonate was added and stirred vigorously for 15 min. The organic phase was removed via the tap and passed over a column of celite/silica then the solvent was removed from the colorless filtrate to yield 90.9 g (93%) of **3** as a white solid.  $^1\text{H NMR}$ , (400 MHz,  $\text{CDCl}_3$ ),  $\delta$  9.91 (s, 1H, CHO), 7.34 (s, 2H, ArH), 5.34 (s, 4H,  $\text{OCH}_2\text{O}$ ), 3.54 (s, 6H,  $\text{OCH}_3$ ), MS:  $m/z$  (ESI, pos.) = 328.9  $[\text{M} + 23]^+$ .

#### 4.2.5. (4-Bromo-3,5-bis-methoxymethoxy-phenyl)-phenyl-methanol

Glassware was dried overnight in a 110 °C oven, assembled hot, and allowed to come to ambient temperature under dry positive nitrogen pressure. A solution of **3** (3.18 g, 10.4 mmol) in 60 mL of anhydrous THF was cooled in an ice bath to which phenyl magnesium bromide (15.6 mL, 15.6 mmol, 1 M solution in THF) was added dropwise. The reaction was stirred at 0 °C for 1 h then allowed to warm to ambient temperature then stirred for an additional 3 h. The reaction was quenched with saturated ammonium chloride (60 mL), layers separated, and the aqueous phase extracted with THF ( $2 \times 50$  mL), and the organic phase extracted with brine (50 mL) then dried over sodium sulfate. Solvent was removed and the residue was loaded onto a SNAP Ultra 50 g silica column and eluted with a hexane:ethyl acetate gradient (5% to 5% 1 column volume, 5% to 40% 10 column volumes, 40% to 40% 2 column volumes). Product fractions were pooled and dried yielding 3.42 g (86%) of the product as a white solid.  $^1\text{H NMR}$ , (400 MHz,  $\text{CDCl}_3$ ),  $\delta$  7.35 (m, 5H, ArH), 6.88 (s, 2H, ArH), 5.77 (d,  $J = 4$  Hz, 1H,  $\text{CHOH}$ ), 5.21 (s, 4H,  $\text{OCH}_2\text{O}$ ), 3.5 (s, 6H,  $\text{OCH}_3$ ), 2.28 (d,  $J = 3.6$  Hz, 1H,  $\text{CHOH}$ ), MS:  $m/z$  (ESI, pos.) = 406.9  $[\text{M} + 23]^+$ .

Utilizing 2-thienyl magnesium (1 M solution in THF) following alcohol was similarly prepared.

#### 4.2.6. (4-Bromo-3,5-bis-methoxymethoxy-phenyl)-thiophen-2-yl-methanol

Pale yellow solid (1.57 g, 70%)  $^1\text{H NMR}$ , (400 MHz,  $\text{CDCl}_3$ ),  $\delta$  7.26 (dd,  $J = 3.2$  Hz, 1.2 Hz, 1H, ThiophenylH), 6.93 (s, 2H, ArH), 6.89 (dt,  $J = 3.3$ , 0.8 Hz, ThiophenylH), 5.97 (d,  $J = 3.6$  Hz, 1H,  $\text{CHOH}$ ), 5.25 (s, 4H,  $\text{OCH}_2\text{O}$ ), 3.49 (s, 6H,  $\text{OCH}_3$ ), 2.74 (d,  $J = 4.0$  Hz, 1H,  $\text{CHOH}$ ), MS:  $m/z$  (ESI, pos.) = 412.9  $[\text{M} + 23]^+$ .

#### 4.2.7. (4-Bromo-3,5-bis-methoxymethoxy-phenyl)-phenyl-methanone (4)

Into a 500 mL flask was charged PCC (3.58 g, 16.7 mmol) and 120 mL of dichloromethane. The mixture was briefly heated to reflux then (4-bromo-3,5-bis-methoxymethoxy-phenyl)-phenyl-methanol (3.04 g, 7.93 mmol) dissolved in 60 mL of dichloromethane was added and stirred for 1 h at ambient temperature. To the mixture was added 150 mL of 1 N sodium hydroxide and the mixture stirred for 45 min. The phases were separated, and the green aqueous phase extracted with dichloromethane ( $2 \times 100$  mL) and combined organic phase dried with sodium sulfate. The solvent was removed and the remaining material was loaded onto a 50 g SNAP Ultra column and eluted with a hexane:ethyl acetate gradient (5% to 5% 1 column volume, 5% to 40% 10 column volumes, 40% to 40% 2 column volumes). Product fractions were pooled and dried yielding 2.72 g (90%) of the product as a white solid.  $^1\text{H NMR}$ , (400 MHz,  $\text{CDCl}_3$ ),  $\delta$  7.81 (d,  $J = 8.4$  Hz, 2H, ArH), 7.60 (t,  $J = 7.4$  Hz, 1H, ArH), 7.50 (t,  $J = 7.6$  Hz, 2H, ArH), 7.24 (s, 2H, ArH), 5.27 (s, 4H,  $\text{OCH}_2\text{O}$ ), 3.51 (s, 6H,  $\text{OCH}_3$ ), MS:  $m/z$  (ESI, pos.) = 404.9  $[\text{M} + 23]^+$ .

The following ketone was similarly prepared.

#### 4.2.8. (4-Bromo-3,5-bis-methoxymethoxy-phenyl)-thiophen-2-yl-methanone (5)

Pale yellow solid (1.07 g, 73%)  $^1\text{H NMR}$ , (400 MHz,  $\text{CDCl}_3$ ),  $\delta$  7.74 (dd,  $J = 4.9$ , 1.0 Hz, 1H, ThiophenylH), 7.67 (dd,  $J = 3.7$ , 1.0 Hz, 1H, ThiophenylH), 7.33 (s, 2H, ArH), 7.18 (dd,  $J = 5.0$ , 3.8 Hz, 1H, ThiophenylH), 5.31 (s, 4H,  $\text{OCH}_2\text{O}$ ), 3.54 (s, 6H,  $\text{OCH}_3$ ), MS:  $m/z$  (ESI, pos.) = 410.7  $[\text{M} + 23]^+$ .

#### 4.2.9. (2,6-Bis-methoxymethoxy-3'-trifluoromethyl-biphenyl-4-yl)-phenyl-methanone (6)

Tetrahydrofuran and 0.5 N K<sub>3</sub>PO<sub>4</sub> were degassed via 3 cycles of evacuation and nitrogen flush with sonication. Into an oven dried reaction tube and stirring bar was charged 4 (42.3 mg, 0.11 mmol), 3-trifluoromethyl phenyl boronic acid (32.6 mg, 0.17 mmol), and Pd-G3 SPhos (1.6 mg, 2 μmol) and the tube was sealed with a septum. The tube was evacuated and flushed with nitrogen 3 times then degassed THF (0.5 mL) followed by 0.5 N tribasic potassium phosphate (2 mL) were added via syringe. The mixture was stirred at ambient temperature for 8 h after which ethyl acetate (5 mL) was added. Phases were separated and the aqueous phase extracted with ethyl acetate (2 × 5 mL), combine organic phase dried with sodium sulfate, and the solvent was removed. The remaining material was loaded onto a 10 g SNAP Ultra column and eluted with a hexane:ethyl acetate gradient (2% to 2% 1 column volume, 2% to 20% 10 column volumes, 20% to 20% 2 column volumes). Product fractions were pooled and dried yielding 38.7 mg (78%) of the product as a colorless viscous oil. <sup>1</sup>H NMR, (400 MHz, CDCl<sub>3</sub>), δ 7.88 (d, *J* = 7.6 Hz, 2H, ArH), 7.81 (d, *J* = 7.6 Hz, 1H, ArH), 7.68 (s, 1H, ArH), 7.59 (m, 3H, ArH), 7.53 (t, *J* = 7.6 Hz, 2H, ArH), 7.31 (s, 2H, ArH), 5.08 (s, 4H, OCH<sub>2</sub>O), 3.07 (s, 6H, OCH<sub>3</sub>), MS: *m/z* (ESI, pos.) = 447.3 [M + 1]<sup>+</sup>.

Utilizing the appropriate aryl/heteroaryl boronic acids the following methanones were prepared.

#### 4.2.10. (3',5'-Difluoro-2,6-bis-methoxymethoxy-biphenyl-4-yl)-phenyl-methanone (7)

Colorless resin (31.8 mg, 72%). <sup>1</sup>H NMR, (400 MHz, CDCl<sub>3</sub>), δ 7.87 (d, *J* = 8.0 Hz, 2H, ArH), 7.63 (t, *J* = 7.2 Hz, 1H, ArH), 7.52 (t, *J* = 8.0 Hz, 2H, ArH), 7.29 (s, 2H, ArH), 6.90 (d, *J* = 7.2 Hz, 2H, ArH), 6.79 (t, *J* = 8.8 Hz, 1H, ArH), 5.1 (s, 4H, OCH<sub>2</sub>O), 3.33 (s, 6H, OCH<sub>3</sub>), MS: *m/z* (ESI, pos.) = 437.3 [M + 23]<sup>+</sup>.

#### 4.2.11. (2',5'-Dichloro-2,6-bis-methoxymethoxy-biphenyl-4-yl)-phenyl-methanone (8)

Colorless resin (17.6 mg, 41%) <sup>1</sup>H NMR, (400 MHz, CDCl<sub>3</sub>), δ 7.88 (d, *J* = 8.0 Hz, 2H, ArH), 7.61 (t, *J* = 7.6 Hz, 1H, ArH), 7.50 (t, *J* = 7.6 Hz, 2H, ArH), 7.42 (d, *J* = 8.4 Hz, 1H, ArH), 7.30 (s, 2H, ArH), 7.28–7.24 (m, 2H, ArH), 5.1 (s, 4H, OCH<sub>2</sub>O), 3.48 (s, 6H, OCH<sub>3</sub>), MS: *m/z* (ESI, pos.) = 447.4 [M + 1]<sup>+</sup>.

#### 4.2.12. (2,6-Bis-methoxymethoxy-3',5'-bis-trifluoromethyl-biphenyl-4-yl)-phenyl-methanone (9)

Off white solid (73.9 mg, 60%) <sup>1</sup>H NMR, (400 MHz, CDCl<sub>3</sub>), δ 7.87 (m, 5H, ArH), 7.62 (t, *J* = 7.6 Hz, 1H, ArH), 7.51 (t, *J* = 7.6 Hz, 2H, ArH), 7.30 (s, 2H, ArH), 5.11 (s, 4H, OCH<sub>2</sub>O), 3.37 (s, 6H, OCH<sub>3</sub>), MS: *m/z* (ESI, pos.) = 515.3 [M + 1]<sup>+</sup>.

#### 4.2.13. (2,6-Bis-methoxymethoxy-3'-methyl-biphenyl-4-yl)-phenyl-methanone (10)

Colorless resin (17.2 mg, 44%) <sup>1</sup>H NMR, (400 MHz, CDCl<sub>3</sub>), δ 7.88 (d, *J* = 8.0 Hz, 2H, ArH), 7.62 (t, *J* = 7.6 Hz, 1H, ArH), 7.50 (m, 5H, ArH), 7.33 (s, 2H, ArH), 7.24 (s, 1H, ArH), 5.06 (s, 4H, OCH<sub>2</sub>O), 3.50 (s, 6H, OCH<sub>3</sub>), 2.41 (s, 3H, Me), MS: *m/z* (ESI, pos.) = 415.3 [M + 23]<sup>+</sup>.

#### 4.2.14. (4-Benzo[1,3]dioxol-5-yl-3,5-bis-methoxymethoxy-phenyl)-phenyl-methanone (11)

Colorless resin (36.4 mg, 81%) <sup>1</sup>H NMR, (400 MHz, CDCl<sub>3</sub>), δ 7.85 (d, *J* = 8.1 Hz, 2H, ArH), 7.58 (t, *J* = 6.4 Hz, 1H, ArH), 7.49 (t, *J* = 8.0 Hz, 2H, ArH), 7.31 (s, 2H, ArH), 6.87 (m, 3H, ArH), 6.00 (s, 2H, ArOCH<sub>2</sub>O), 5.07 (s, 4H, OCH<sub>2</sub>O), 3.38 (s, 6H, OCH<sub>3</sub>), MS: *m/z* (ESI, pos.) = 445.2 [M + 23]<sup>+</sup>.

#### 4.2.15. [4-(2,3-Dihydro-benzo[1,4]dioxin-6-yl)-3,5-bis-methoxymethoxy-phenyl]-phenyl-methanone (12)

White solid (21.7 mg, 43%) <sup>1</sup>H NMR, (400 MHz, CDCl<sub>3</sub>), δ 7.86 (d, *J*

= 7.6 Hz, 2H, ArH), 7.59 (t, *J* = 7.6 Hz, 1H, ArH), 7.49 (t, *J* = 7.6 Hz, 2H, ArH), 7.31 (s, 2H, ArH), 6.93 (d, *J* = 8.8 Hz, 1H, ArH), 6.91 (s, 1H, ArH), 6.87 (d, *J* = 8.8 Hz, 1H, ArH), 5.08 (s, 4H, OCH<sub>2</sub>O), 4.31 (s, 4H, ArOCH<sub>2</sub>CH<sub>2</sub>O), 3.34 (s, 6H, OCH<sub>3</sub>), MS: *m/z* (ESI, pos.) = 437.5 [M + 1]<sup>+</sup>.

#### 4.2.16. (3'-Hydroxymethyl-2,6-bis-methoxymethoxy-biphenyl-4-yl)-phenyl-methanone (13)

White solid (20.8 mg, 42%) <sup>1</sup>H NMR, (400 MHz, CDCl<sub>3</sub>), δ 7.87 (d, *J* = 7.6 Hz, 2H, ArH), 7.62 (t, *J* = 7.2 Hz, 1H, ArH), 7.50 (t, *J* = 7.6 Hz, 2H, ArH), 7.41 (t, *J* = 6.0 Hz, 1H, ArH), 7.39 (m, 2H, ArH), 7.33 (t, *J* = 1.6 Hz, 1H, ArH), 7.31 (s, 2H, ArH), 5.05 (s, 4H, OCH<sub>2</sub>O), 4.75 (s, 2H, CH<sub>2</sub>OH), 3.38 (s, 6H, OCH<sub>3</sub>), MS: *m/z* (ESI, pos.) = 431.1 [M + 23]<sup>+</sup>.

#### 4.2.17. 4'-Benzoyl-4-fluoro-2',6'-bis-methoxymethoxy-biphenyl-3-carbonitrile (14)

White solid (29.3 mg, 21%) <sup>1</sup>H NMR, (400 MHz, CDCl<sub>3</sub>), δ 7.87 (d, *J* = 8.0 Hz, 2H, ArH), 7.63 (m, 3H, ArH), 7.52 (t, *J* = 7.6 Hz, 2H, ArH), 7.30 (s, 2H, ArH), 7.23 (s, 1H, ArH), 5.06 (s, 4H, OCH<sub>2</sub>O), 3.38 (s, 6H, OCH<sub>3</sub>), MS: *m/z* (ESI, pos.) = 444.3 [M + 23]<sup>+</sup>.

#### 4.2.18. (3,5-Bis-methoxymethoxy-4-pyridin-3-yl-phenyl)-phenyl-methanone (15)

White solid (18.3 mg, 45%) <sup>1</sup>H NMR, (400 MHz, CDCl<sub>3</sub>), δ 8.65 (d, *J* = 2.0 Hz, 1H, PyridylH), 8.59 (dd, *J* = 4.8, 1.6 Hz, 1H, PyridylH), 7.88 (d, *J* = 8.0 Hz, 2H, ArH), 7.74 (dt, *J* = 8.0, 1.6 Hz, 1H, PyridylH), 7.61 (t, *J* = 7.2 Hz, 1H, ArH), 7.52 (t, *J* = 6.4, 2H, ArH), 7.39 (dd, *J* = 7.6, 2.8 Hz, 1H, PyridylH), 7.33 (s, 2H, ArH), 5.10 (s, 4H, OCH<sub>2</sub>O), 3.38 (s, 6H, OCH<sub>3</sub>), MS: *m/z* (ESI, pos.) = 380.1 [M + 1]<sup>+</sup>.

#### 4.2.19. [4-(2-Fluoro-pyridin-4-yl)-3,5-bis-methoxymethoxy-phenyl]-phenyl-methanone (16)

White solid (13.8 mg, 27%) <sup>1</sup>H NMR, (400 MHz, CDCl<sub>3</sub>), δ 8.27 (d, *J* = 5.2 Hz, 1H, PyridylH), 7.86 (d, *J* = 8.0 Hz, 2H, ArH), 7.60 (t, *J* = 7.2 Hz, 1H, ArH), 7.51 (t, *J* = 7.2 Hz, 2H, ArH), 7.30 (s, 2H, ArH), 7.22 (dt, *J* = 5.2, 1.2 Hz, 1H, PyridylH), 6.99 (s, 1H, PyridylH), 5.11 (s, 4H, OCH<sub>2</sub>O), 3.34 (s, 6H, OCH<sub>3</sub>), MS: *m/z* (ESI, pos.) = 420.2 [M + 23]<sup>+</sup>.

#### 4.2.20. [4-(2-Chloro-pyridin-4-yl)-3,5-bis-methoxymethoxy-phenyl]-phenyl-methanone (17)

White solid (7.1 mg, 17%) <sup>1</sup>H NMR, (400 MHz, CDCl<sub>3</sub>), δ 8.45 (d, *J* = 4.4 Hz, 1H, PyridylH), 7.86 (d, *J* = 8.0 Hz, 2H, ArH), 7.62 (t, *J* = 7.6 Hz, 1H, ArH), 7.52 (t, *J* = 8.0 Hz, 2H, ArH), 7.38 (s, 1H, PyridylH), 7.29 (s, 2H, ArH), 7.26 (m, 1H, PyridylH), 5.11 (s, 4H, OCH<sub>2</sub>O), 3.34 (s, 6H, OCH<sub>3</sub>), MS: *m/z* (ESI, pos.) = 414.2 [M + 1]<sup>+</sup>.

#### 4.2.21. (3,5-Bis-methoxymethoxy-4-thiophen-3-yl-phenyl)-phenyl-methanone (18)

Colorless viscous oil (12.1 mg, 33%) <sup>1</sup>H NMR, (400 MHz, CDCl<sub>3</sub>), δ 7.86 (d, *J* = 8.4 Hz, 2H, ArH), 7.62 (t, *J* = 7.6 Hz, 1H, ArH), 7.52 (m, 3H, ArH/thiophenylH), 7.35 (m, 2H, thiophenylH), 7.31 (s, 2H, ArH), 5.15 (s, 4H, OCH<sub>2</sub>O), 3.37 (s, 6H, OCH<sub>3</sub>), MS: *m/z* (ESI, pos.) = 385.3 [M + 1]<sup>+</sup>.

#### 4.2.22. (4-Furan-3-yl-3,5-bis-methoxymethoxy-phenyl)-phenyl-methanone (19)

Colorless viscous oil (29.5 mg, 71%) <sup>1</sup>H NMR, (400 MHz, CDCl<sub>3</sub>), δ 7.97 (s, 1H, FuranylH), 7.84 (d, *J* = 8.0 Hz, 2H, ArH), 7.61 (t, *J* = 7.2 Hz, 1H, ArH), 7.48 (m, 3H, ArH/furanylH), 7.31 (s, 2H, ArH), 6.97 (s, 1H, FuranylH), 5.19 (s, 4H, OCH<sub>2</sub>O), 3.43 (s, 6H, OCH<sub>3</sub>), MS: *m/z* (ESI, pos.) = 369.3 [M + 1]<sup>+</sup>.

#### 4.2.23. (2,6-Bis-methoxymethoxy-3'-trifluoromethyl-biphenyl-4-yl)-thiophen-2-yl-methanone (34)

Pale yellow resin (34.4 mg, 71%) <sup>1</sup>H NMR, (400 MHz, CDCl<sub>3</sub>), δ 7.76–7.73 (m, 3H, ArH/ThiophenylH), 7.67 (s, 1H, ArH), 7.61 (m, 2H,

ArH), 7.33 (s, 2H, ArH), 7.19 (m, 1H, ThiophenylH), 5.11 (s, 4H, OCH<sub>2</sub>O), 3.38 (s, 6H, OCH<sub>3</sub>), MS: *m/z* (ESI, pos.) = 475.3 [M + 23]<sup>+</sup>.

#### 4.2.24. (2,6-Bis-methoxymethoxy-3'-methyl-biphenyl-4-yl)-thiophen-2-yl-methanone (35)

Pale yellow solid (34.1 mg, 79%) <sup>1</sup>H NMR, (400 MHz, CDCl<sub>3</sub>), δ 7.75 (dd, *J* = 3.6, 1.2 Hz, 1H, ThiophenylH), 7.72 (dd, *J* = 5.2, 1.2 Hz, 1H, ThiophenylH), 7.40 (s, 2H, ArH), 7.33 (t, *J* = 6.6 Hz, 1H, ArH), 7.18 (m, 4H, ArH/thiophenylH), 5.08 (s, 4H, OCH<sub>2</sub>O), 3.39 (s, 6H, OCH<sub>3</sub>), 2.48 (s, 3H, Me), MS: *m/z* (ESI, pos.) = 399.3 [M + 1]<sup>+</sup>.

#### 4.2.25. (2,6-Bis-methoxymethoxy-3',5'-bis-trifluoromethyl-biphenyl-4-yl)-thiophen-2-yl-methanone (36)

Pale yellow solid (14.7 mg, 25%) <sup>1</sup>H NMR, (400 MHz, CDCl<sub>3</sub>), δ 7.88 (s, 3H, ArH), 7.76 (dd, *J* = 5.0, 1.2 Hz, 1H, ThiophenylH), 7.74 (dd, *J* = 3.8 Hz, 1.2 Hz, 1H, ThiophenylH), 7.39 (s, 2H, ArH), 7.20 (dd, *J* = 5.0, 3.6 Hz, 1H, ThiophenylH), 5.14 (s, 4H, OCH<sub>2</sub>O), 3.36 (s, 6H, OCH<sub>3</sub>), MS: *m/z* (ESI, pos.) = 543.1 [M + 23]<sup>+</sup>.

#### 4.2.26. (2',5'-Dichloro-2,6-bis-methoxymethoxy-biphenyl-4-yl)-thiophen-2-yl-methanone (37)

Pale yellow resin (29.6 mg, 59%) <sup>1</sup>H NMR, (400 MHz, CDCl<sub>3</sub>), δ 7.75 (overlapping dd, *J* = 4.8, 1.2 Hz, 2H, ThiophenylH), 7.42 (d, *J* = 8.4 Hz, 1H, ArH), 7.39 (s, 2H, ArH), 7.33–7.26 (m, 2H, ArH), 7.19 (dd, *J* = 5.2, 3.8 Hz, 1H, ThiophenylH), 5.12 (s, 4H, OCH<sub>2</sub>O), 3.36 (s, 6H, OCH<sub>3</sub>), MS: *m/z* (ESI, pos.) = 475.1 [M + 23]<sup>+</sup>.

#### 4.2.27. (3'-Hydroxymethyl-2,6-bis-methoxymethoxy-biphenyl-4-yl)-thiophen-2-yl-methanone (38)

Pale yellow resin (12.5 mg, 29%) <sup>1</sup>H NMR, (400 MHz, CDCl<sub>3</sub>), δ 7.75 (dd, *J* = 4.0, 1.2 Hz, 1H, ThiophenylH), 7.37 (dd, *J* = 4.8, 1.2 Hz, 1H, ThiophenylH), 7.44 (t, *J* = 8.4 Hz, 1H, ArH), 7.40 (s, 2H, ArH), 7.38 (m, 2H, ArH), 7.31 (d, *J* = 7.6 Hz, 1H, ArH), 7.19 (dd, *J* = 5.0, 3.8 Hz, 1H, ThiophenylH), 5.09 (s, 4H, OCH<sub>2</sub>O), 4.76 (s, 2H, CH<sub>2</sub>OH), 3.36 (s, 6H, OCH<sub>3</sub>), MS: *m/z* (ESI, pos.) = 437.1 [M + 23]<sup>+</sup>.

#### 4.2.28. (3,5-Bis-methoxymethoxy-4-pyridin-3-yl-phenyl)-thiophen-2-yl-methanone (39)

Pale yellow resin (18.6 mg, 47%) <sup>1</sup>H NMR, (400 MHz, CDCl<sub>3</sub>), δ 8.65 (dd, *J* = 2.0, 0.4 Hz, 1H, PyridylH), 8.59 (dd, *J* = 4.8, 2.0 Hz, 1H, PyridylH), 7.75 (m, 3H, PyridylH/ThiophenylH), 7.41 (s, 2H, ArH), 7.39 (dd, *J* = 7.9, 0.8 Hz, 1H, PyridylH), 7.20 (dd, *J* = 5.0, 4.0 Hz, 1H, ThiophenylH), 5.12 (s, 4H, OCH<sub>2</sub>O), 3.35 (s, 6H, OCH<sub>3</sub>), MS: *m/z* (ESI, pos.) = 408.0 [M + 23]<sup>+</sup>.

#### 4.2.29. (2,6-Dihydroxy-3'-trifluoromethyl-biphenyl-4-yl)-phenyl-methanone (20)

To a suspension of **6** (38.7 mg, 86.7 μmol) in methanol (3 mL) was added 3 N hydrochloric acid in methanol (0.5 mL) and the mixture heated to reflux. The solids dissolved in 1 h and after 2 h water (5 mL) and ethyl acetate (5 mL) were added, phases separated, and the aqueous phase extracted with ethyl acetate (2 × 5 mL) and organic phase dried with sodium sulfate. The solvent was removed and the residue applied to a 10 g SNAP Ultra column and eluted with a hexane:ethyl acetate gradient (5% to 5% 1 column volume, 5% to 40% 10 column volumes, 40% to 40% 2 column volumes). Product fractions were pooled and dried yielding 28.2 mg (91%) of the product as a colorless glass. Analytical UPLC retention time 2.90 min; purity 98.2%. <sup>1</sup>H NMR, (400 MHz, (CD<sub>3</sub>)<sub>2</sub>CO), δ 7.84–7.78 (m, 4H, ArH), 7.67 (m, 3H, ArH), 7.57 (t, *J* = 6.8 Hz, 2H, ArH), 6.98 (s, 2H, ArH). <sup>13</sup>C NMR, (100 MHz, (CD<sub>3</sub>)<sub>2</sub>CO), δ 195.8, 156.2, 139.1, 138.7, 135.9, 135.7, 133.1, 130.4, 130.1, 129.3, 129.1, 128.4, 128.4, 124.4, 109.7. HRMS: *m/z* calculated for C<sub>20</sub>H<sub>14</sub>F<sub>3</sub>O<sub>3</sub>, [M+H]<sup>+</sup> 359.0895, found: 359.0892.

The following resorcinols were similarly prepared.

#### 4.2.30. (3',5'-Difluoro-2,6-dihydroxy-biphenyl-4-yl)-phenyl-methanone (21)

Off white solid (14.9 mg, 60%) Analytical UPLC retention time 2.68 min; purity 99.8%. <sup>1</sup>H NMR, (400 MHz, (CD<sub>3</sub>)<sub>2</sub>CO), δ 7.81 (d, *J* = 8.4 Hz, 2H, ArH), 7.67 (t, *J* = 7.4, 1H, ArH), 7.57 (t, *J* = 7.7 Hz, 2H, ArH), 7.13 (m, 2H, Ar'H), 6.97 (t, *J* = 9.1 Hz, 1H, Ar'H), 6.96 (s, 2H, ArH). <sup>13</sup>C NMR (100 MHz, (CD<sub>3</sub>)<sub>2</sub>CO), δ 195.8, 164.6, 164.5, 162.2, 161.1, 156.1, 139.3, 138.6, 138.5, 133.1, 130.4, 129.1, 118.9, 114.8, 114.7, 114.6, 109.6, 103.1, 102.8, 102.6. HRMS: *m/z* calculated for C<sub>19</sub>H<sub>13</sub>O<sub>3</sub>F<sub>2</sub>, [M+H]<sup>+</sup> 327.0833, found: 327.0834.

#### 4.2.31. (2',5'-Dichloro-2,6-dihydroxy-biphenyl-4-yl)-phenyl-methanone (22)

Off white solid (10.6 mg, 70%) Analytical UPLC retention time 3.31 min; purity 100%. <sup>1</sup>H NMR, (400 MHz, (CD<sub>3</sub>)<sub>2</sub>CO), δ 7.81 (d, *J* = 8.4 Hz, 2H, ArH), 7.67 (t, *J* = 7.5, 1H, ArH), 7.55 (m, 3H, ArH), 7.41 (m, 2H, ArH), 6.94 (s, 2H, ArH). <sup>13</sup>C NMR (100 MHz, (CD<sub>3</sub>)<sub>2</sub>CO), δ 195.9, 156.5, 139.8, 138.7, 136.5, 134.2, 133.13, 133.1, 132.5, 131.5, 130.4, 129.7, 129.2, 118.1, 109.6. HRMS: *m/z* calculated for C<sub>19</sub>H<sub>13</sub>O<sub>3</sub>Cl<sub>2</sub>, [M+H]<sup>+</sup> 359.0242, found: 359.0247.

#### 4.2.32. (2,6-Dihydroxy-3',5'-bis-trifluoromethyl-biphenyl-4-yl)-phenyl-methanone (23)

White solid (16.0 mg, 59%) Analytical UPLC retention time 3.91 min; purity 100%. <sup>1</sup>H NMR, (400 MHz, (CD<sub>3</sub>)<sub>2</sub>CO), δ 8.15 (s, 2H, Ar'H), 7.99 (s, 1H, Ar'H), 7.83 (d, *J* = 7.0, 1H, ArH), 7.68 (t, *J* = 7.4 Hz, 1H, ArH), 7.57 (t, *J* = 7.3 Hz, 2H, ArH), 7.00 (s, 2H, ArH). <sup>13</sup>C NMR (100 MHz, (CD<sub>3</sub>)<sub>2</sub>CO), δ 195.8, 156.2, 139.9, 138.5, 137.6, 133.3, 132.5, 131.5, 131.2, 130.5, 129.2, 126.1, 121.33, 121.3, 117.9, 109.7. HRMS: *m/z* calculated for C<sub>21</sub>H<sub>13</sub>O<sub>3</sub>F<sub>6</sub>, [M+H]<sup>+</sup> 427.0769, found: 427.0777.

#### 4.2.33. (2,6-Dihydroxy-3'-methyl-biphenyl-4-yl)-phenyl-methanone (24)

White solid (11.6 mg, 87%) Analytical UPLC retention time 3.20 min; purity 100%. <sup>1</sup>H NMR, (400 MHz, (CD<sub>3</sub>)<sub>2</sub>CO), δ 7.81 (d, *J* = 7.6 Hz, 2H, ArH), 7.65 (t, *J* = 7.3, 1H, ArH), 7.56 (t, *J* = 7.3 Hz, 2H, ArH), 7.27 (m, 3H, Ar'H), 7.14 (d, *J* = 7.4 Hz, 1H, Ar'H), 6.95 (s, 2H, ArH), 2.37 (s, 3H, CH<sub>3</sub>Ar). <sup>13</sup>C NMR (100 MHz, (CD<sub>3</sub>)<sub>2</sub>CO), δ 196.0, 156.3, 138.9, 138.4, 138.0, 134.4, 133.0, 132.3, 130.4, 129.1, 128.8, 128.7, 121.7, 109.7, 21.5. HRMS: *m/z* calculated for C<sub>20</sub>H<sub>17</sub>O<sub>3</sub>, [M+H]<sup>+</sup> 305.1178, found: 305.1185.

#### 4.2.34. (4-Benzo[1,3]dioxol-5-yl-3,5-dihydroxy-phenyl)-phenyl-methanone (25)

White solid (16.8 mg, 58%) Analytical UPLC retention time 2.49 min; purity 99.4%. <sup>1</sup>H NMR, (400 MHz, (CD<sub>3</sub>)<sub>2</sub>CO), δ 7.81 (d, *J* = 7.8 Hz, 2H, ArH), 7.66 (t, *J* = 7.4, 1H, ArH), 7.56 (t, *J* = 7.5 Hz, 2H, ArH), 6.96–6.89 (m, 3H, Ar'H), 6.94 (s, 2H, ArH), 6.03 (s, 2H, Ar'OCH<sub>2</sub>O). <sup>13</sup>C NMR (100 MHz, (CD<sub>3</sub>)<sub>2</sub>CO), δ 195.9, 156.4, 148.3, 147.7, 138.9, 138.3, 133.0, 130.4, 129.1, 127.8, 125.2, 112.1, 109.7, 108.7, 101.9. HRMS: *m/z* calculated for C<sub>20</sub>H<sub>15</sub>O<sub>5</sub>, [M+H]<sup>+</sup> 335.0919, found: 335.0916.

#### 4.2.35. [4-(2,3-Dihydro-benzo[1,4]dioxin-6-yl)-3,5-dihydroxy-phenyl]-phenyl-methanone (26)

White solid (16.7 mg, 96%) Analytical UPLC retention time 2.41 min; purity 98.2%. <sup>1</sup>H NMR, (400 MHz, (CD<sub>3</sub>)<sub>2</sub>CO), δ 7.81 (d, *J* = 7.2 Hz, 2H, ArH), 7.66 (t, *J* = 7.4, 1H, ArH), 7.56 (t, *J* = 7.6 Hz, 2H, ArH), 6.94 (t, *J* = 1.8, 1H, Ar'H), 6.93 (s, 2H, ArH), 6.92 (t, *J* = 2 Hz, 1H, Ar'H), 6.86 (d, *J* = 8.3, 1H, Ar'H), 2.85 (m, 4H, Ar'OCH<sub>2</sub>CH<sub>2</sub>O). <sup>13</sup>C NMR (100 MHz, (CD<sub>3</sub>)<sub>2</sub>CO), δ 195.9, 170.9, 156.3, 144.2, 143.9, 138.9, 138.3, 132.9, 130.4, 129.1, 127.1, 124.8, 120.5, 117.4, 109.6, 65.3, 65.1. HRMS: *m/z* calculated for C<sub>21</sub>H<sub>17</sub>O<sub>5</sub>, [M+H]<sup>+</sup> 349.1076, found: 349.1074.

#### 4.2.36. (2,6-Dihydroxy-3'-hydroxymethyl-biphenyl-4-yl)-phenyl-methanone (27)

White solid (8.2 mg, 54%) Analytical UPLC retention time 2.09 min;

purity 95.4%.  $^1\text{H}$  NMR, (400 MHz,  $(\text{CD}_3)_2\text{CO}$ ),  $\delta$  7.82 (d,  $J = 7.8$  Hz, 2H, ArH), 7.66 (t,  $J = 7.5$ , 1H, ArH), 7.56 (t,  $J = 7.7$  Hz, 2H, ArH), 7.45 (s, 1H, Ar'H), 7.40–7.32 (m, 3H, Ar'H), 6.94, (s, 2H, ArH), 4.68 (s, 2H,  $\text{CH}_2\text{OH}$ ).  $^{13}\text{C}$  NMR (100 MHz,  $(\text{CD}_3)_2\text{CO}$ ),  $\delta$  196.0, 156.3, 142.9, 138.9, 138.5, 134.4, 133.0, 130.4, 130.2, 129.9, 129.1, 128.5, 126.3, 121.7, 109.7, 64.8. HRMS:  $m/z$  calculated for  $\text{C}_{20}\text{H}_{17}\text{O}_4$ ,  $[\text{M}+\text{H}]^+$  321.1127, found: 321.1114.

#### 4.2.37. 4'-Benzoyl-4-fluoro-2',6'-dihydroxy-biphenyl-3-carbonitrile (28)

White solid (3.2 mg, 26%) Analytical UPLC retention time 2.52 min; purity 98%.  $^1\text{H}$  NMR, (400 MHz,  $(\text{CD}_3)_2\text{CO}$ ),  $\delta$  7.91 (m, 2H, Ar'H), 7.81 (d,  $J = 7.6$ , 2H, ArH), 7.67 (t,  $J = 7.2$  Hz, 1H, ArH), 7.57 (t,  $J = 7.6$ , 2H, ArH), 7.48 (t,  $J = 9.2$  Hz, 1H, Ar'H), 6.97 (s, 2H, ArH).  $^{13}\text{C}$  NMR (100 MHz,  $(\text{CD}_3)_2\text{CO}$ ),  $\delta$  195.7, 156.2, 139.4, 139.38, 139.3, 138.6, 136.9, 133.2, 130.5, 129.2, 116.7, 116.5, 109.7, 79.3, 79.0. HRMS:  $m/z$  calculated for  $\text{C}_{20}\text{H}_{13}\text{FNO}_3$ ,  $[\text{M}+\text{H}]^+$  334.0879, found: 334.0871.

#### 4.2.38. (3,5-Dihydroxy-4-pyridin-3-yl-phenyl)-phenyl-methanone (29)

White solid (11.5 mg, 85%) Analytical UPLC retention time 2.32 min; purity 96.2%.  $^1\text{H}$  NMR, (400 MHz,  $(\text{CD}_3)_2\text{CO}$ ),  $\delta$  8.70 (d,  $J = 2.2$  Hz, 1H, PyridylH), 8.50 (dd,  $J = 4.9$  Hz, 1.7 Hz, 1H, PyridylH), 7.88 (dt,  $J = 7.7$  Hz, 2.1 Hz, 1H, PyridylH), 7.82 (d,  $J = 7.8$ , 2H, ArH), 7.66 (t,  $J = 7.4$  Hz, 1H, ArH), 7.56 (t,  $J = 7.7$ , 2H, ArH), 7.41 (dd,  $J = 8.0$  Hz, 2.8, 1H, PyrH), 6.98 (s, 2H, ArH).  $^{13}\text{C}$  NMR (100 MHz,  $(\text{CD}_3)_2\text{CO}$ ),  $\delta$  195.9, 157.9, 156.5, 152.3, 148.6, 139.2, 139.0, 138.7, 133.1, 130.8, 130.5, 129.2, 123.6, 118.0, 109.6. HRMS:  $m/z$  calculated for  $\text{C}_{18}\text{H}_{14}\text{NO}_3$ ,  $[\text{M}+\text{H}]^+$  292.0974, found: 292.0966.

#### 4.2.39. [4-(2-Fluoro-pyridin-4-yl)-3,5-dihydroxy-phenyl]-phenyl-methanone (30)

White solid (3.6 mg, 20%) Analytical UPLC retention time 2.67 min; purity 95.6%.  $^1\text{H}$  NMR, (400 MHz,  $(\text{CD}_3)_2\text{CO}$ ),  $\delta$  8.43 (d,  $J = 5.2$  Hz, 1H, PyridylH), 7.82 (d,  $J = 7.8$ , 2H, ArH), 7.68 (t,  $J = 7.2$  Hz, 1H, ArH), 7.57 (m, 3H, ArH/PyridylH), 7.52 (dd,  $J = 5.0$  Hz, 1.5, 1H, PyridylH), 6.96 (s, 2H, ArH).  $^{13}\text{C}$  NMR (100 MHz,  $(\text{CD}_3)_2\text{CO}$ ),  $\delta$  195.7, 156.2, 151.4, 149.8, 146.6, 138.5, 133.3, 130.5, 129.2, 126.9, 126.0, 109.6. HRMS:  $m/z$  calculated for  $\text{C}_{18}\text{H}_{13}\text{NO}_3\text{F}$ ,  $[\text{M}+\text{H}]^+$  310.0879, found: 310.0890.

#### 4.2.40. [4-(2-Chloro-pyridin-4-yl)-3,5-dihydroxy-phenyl]-phenyl-methanone (31)

White solid (3.6 mg, 20%) Analytical UPLC retention time 2.51 min; purity 97.0%.  $^1\text{H}$  NMR, (400 MHz,  $(\text{CD}_3)_2\text{CO}$ ),  $\delta$  8.25 (d,  $J = 5.6$  Hz, 1H, PyridylH), 7.82 (d,  $J = 7.2$ , 2H, ArH), 7.67 (t,  $J = 7.6$  Hz, 1H, ArH), 7.57 (t,  $J = 7.2$  Hz, 2H, ArH), 7.46 (d,  $J = 5.0$  Hz, 1H, PyridylH), 7.19 (s, 1H, PyridylH) 6.97 (s, 2H, ArH).  $^{13}\text{C}$  NMR (100 MHz,  $(\text{CD}_3)_2\text{CO}$ ),  $\delta$  195.7, 156.2, 147.6, 146.2, 138.5, 133.3, 130.5, 129.2, 125.0, 109.6. HRMS:  $m/z$  calculated for  $\text{C}_{18}\text{H}_{13}\text{NO}_3\text{Cl}$ ,  $[\text{M}+\text{H}]^+$  326.0584, found: 326.0578.

#### 4.2.41. (3,5-Dihydroxy-4-thiophen-3-yl-phenyl)-phenyl-methanone (32)

Off white solid (5.9 mg, 64%) Analytical UPLC retention time 2.99 min; purity 100%.  $^1\text{H}$  NMR, (400 MHz,  $(\text{CD}_3)_2\text{CO}$ ),  $\delta$  7.80 (d,  $J = 7.4$ , 2H, ArH), 7.72 (dd,  $J = 2.9$ , 1.3 Hz, 1H, ThiophenylH), 7.65 (t,  $J = 7.3$  Hz, 1H, ArH), 7.56 (t,  $J = 7.6$  Hz, 2H, ArH), 7.51 (dd,  $J = 5.2$ , 1.2 Hz, 1H, ThiophenylH), 7.45 (dd,  $J = 5.0$ , 3.0 Hz, 1H, ThiophenylH), 6.96 (s, 2H, ArH).  $^{13}\text{C}$  NMR (100 MHz,  $(\text{CD}_3)_2\text{CO}$ ),  $\delta$  195.8, 156.4, 138.9, 138.0, 133.7, 132.9, 131.2, 130.4, 129.1, 126.4, 124.1, 109.9. HRMS:  $m/z$  calculated for  $\text{C}_{17}\text{H}_{13}\text{O}_3\text{S}$ ,  $[\text{M}+\text{H}]^+$  297.0585, found: 297.0584.

#### 4.2.42. 4.2.42 (4-Furan-3-yl-3,5-dihydroxy-phenyl)-phenyl-methanone (33)

Off white solid (13.4 mg, 60%). Analytical UPLC retention time 2.96 min; purity 96.1%.  $^1\text{H}$  NMR, (400 MHz,  $(\text{CD}_3)_2\text{CO}$ ),  $\delta$  8.21 (s, 1H, FuranylH), 7.79 (d,  $J = 7.2$ , 2H, ArH), 7.65 (t,  $J = 7.3$  Hz, 1H, ArH), 7.59–7.53 (m, 3H, ArH/FuranylH), 7.26 (d,  $J = 2$  Hz, 1H, FuranylH), 6.97 (s, 2H, ArH).  $^{13}\text{C}$  NMR (100 MHz,  $(\text{CD}_3)_2\text{CO}$ ),  $\delta$  195.8, 156.4, 144.5,

141.9, 139.0, 137.0, 132.9, 130.4, 129.1, 118.6, 109.9. HRMS:  $m/z$  calculated for  $\text{C}_{17}\text{H}_{13}\text{O}_4$ ,  $[\text{M}+\text{H}]^+$  281.0814, found: 281.0819.

#### 4.2.43. (2,6-Dihydroxy-3'-trifluoromethyl-biphenyl-4-yl)-thiophen-2-yl-methanone (40)

Pale yellow solid (18.3 mg, 66%). Analytical UPLC retention time 2.81 min; purity 98.8%.  $^1\text{H}$  NMR, (400 MHz,  $(\text{CD}_3)_2\text{CO}$ ),  $\delta$  8.00 (dd,  $J = 4.8$ , 1.0 Hz, 1H, ThiophenylH), 7.83 (dd,  $J = 3.7$ , 1.0 Hz, 1H, ThiophenylH), 7.80 (m, 2H, Ar'H), 7.66 (m, 2H, Ar'H), 7.29 (dd,  $J = 4.8$ , 3.8 Hz, 1H, ThiophenylH), 7.09 (s, 2H, ArH).  $^{13}\text{C}$  NMR (100 MHz,  $(\text{CD}_3)_2\text{CO}$ ),  $\delta$  187.4, 170.9, 156.4, 156.3, 144.3, 139.6, 135.9, 135.8, 135.7, 135.5, 135.4, 130.5, 130.1, 129.4, 129.1, 128.5, 128.4, 126.9, 124.5, 124.4, 124.3, 124.2119.6, 108.5. HRMS:  $m/z$  calculated for  $\text{C}_{18}\text{H}_{12}\text{O}_3\text{F}_3\text{S}$ ,  $[\text{M}+\text{H}]^+$  365.0459, found: 365.0468.

#### 4.2.44. (2,6-Dihydroxy-3'-methyl-biphenyl-4-yl)-thiophen-2-yl-methanone (41)

Pale yellow solid (17.3 mg, 65%). Analytical UPLC retention time 2.64 min; purity 98.1%.  $^1\text{H}$  NMR, (400 MHz,  $(\text{CD}_3)_2\text{CO}$ ),  $\delta$  7.98 (dd,  $J = 5.0$ , 1.0 Hz, 1H, ThiophenylH), 7.82 (dd,  $J = 4.0$ , 1.0 Hz, 1H, ThiophenylH), 7.33–7.23 (m, 4H, Ar'H/ThiophenylH), 7.14 (d,  $J = 7.4$  Hz, 1H, Ar'H), 7.05 (s, 2H, ArH), 2.37 (s, 3H, Ar'CH<sub>3</sub>).  $^{13}\text{C}$  NMR (100 MHz,  $(\text{CD}_3)_2\text{CO}$ ),  $\delta$  187.5, 156.4, 144.4, 138.9, 138.0, 135.4, 135.1, 134.3, 132.3, 129.8, 128.5, 128.7, 128.6, 121.6, 108.9, 21.5. HRMS:  $m/z$  calculated for  $\text{C}_{18}\text{H}_{15}\text{O}_3\text{S}$ ,  $[\text{M}+\text{H}]^+$  311.0742, found: 311.0707.

#### 4.2.45. (2,6-Dihydroxy-3',5'-bis-trifluoromethyl-biphenyl-4-yl)-thiophen-2-yl-methanone (42)

Pale yellow solid (13.1 mg, 96%). Analytical UPLC retention time 3.11 min; purity 99.3%.  $^1\text{H}$  NMR, (400 MHz,  $(\text{CD}_3)_2\text{CO}$ ),  $\delta$  8.16 (s, 2H, Ar'H), 8.02 (dd,  $J = 5.0$ , 1.1 Hz, 1H, ThiophenylH), 7.99 (s, 1H, Ar'H), 7.83 (dd,  $J = 3.8$ , 1.0 Hz, 1H, ThiophenylH), 7.30 (dd,  $J = 5.0$ , 3.8 Hz, 1H, ThiophenylH), 7.10 (s, 2H, ArH).  $^{13}\text{C}$  NMR (100 MHz,  $(\text{CD}_3)_2\text{CO}$ ),  $\delta$  187.3, 170.9, 156.3, 144.2, 140.4, 137.6, 135.7, 135.6, 132.5, 131.8, 131.5, 131.2, 130.9, 129.2, 126.1, 123.4, 121.4, 121.3, 121.2, 117.8, 108.9. HRMS:  $m/z$  calculated for  $\text{C}_{19}\text{H}_{11}\text{O}_3\text{F}_6\text{S}$ ,  $[\text{M}+\text{H}]^+$  433.0333, found: 433.0334.

#### 4.2.46. (2',5'-Dichloro-2,6-dihydroxy-biphenyl-4-yl)-thiophen-2-yl-methanone (43)

Pale yellow solid (24.3 mg, 98%). Analytical UPLC retention time 2.72 min; purity 97.9%.  $^1\text{H}$  NMR, (400 MHz,  $(\text{CD}_3)_2\text{CO}$ ),  $\delta$  7.99 (dd,  $J = 4.9$ , 1.0 Hz, 1H, ThiophenylH), 7.82 (dd,  $J = 3.8$ , 1.1 Hz, 1H, ThiophenylH), 7.54 (dd,  $J = 6.5$ , 2.4 Hz, 1H, Ar'H), 7.42 (dd,  $J = 7.2$ , 2.4 Hz, 2H, Ar'H), 7.29 (dd,  $J = 5.0$ , 3.8, Hz, 1H, ThiophenylH), 7.05 (s, 2H, ArH).  $^{13}\text{C}$  NMR (100 MHz,  $(\text{CD}_3)_2\text{CO}$ ),  $\delta$  187.4, 170.9, 156.5, 144.3, 140.3, 136.5, 135.6, 135.4, 134.2, 133.1, 132.5, 131.5, 129.7, 129.1, 117.9, 108.5. HRMS:  $m/z$  calculated for  $\text{C}_{17}\text{H}_{11}\text{O}_3\text{SCl}_2$ ,  $[\text{M}+\text{H}]^+$  364.9806, found: 364.9796.

#### 4.2.47. (2,6-Dihydroxy-3'-hydroxymethyl-biphenyl-4-yl)-thiophen-2-yl-methanone (44)

Pale yellow solid (7.2 mg, 73%). Analytical UPLC retention time 2.16 min; purity 99.8%.  $^1\text{H}$  NMR, (400 MHz,  $(\text{CD}_3)_2\text{CO}$ ),  $\delta$  7.98 (dd,  $J = 5.0$ , 1.0 Hz, 1H, ThiophenylH), 7.83 (dd,  $J = 3.8$ , 1.1 Hz, 1H, ThiophenylH), 7.45 (s, 1H, Ar'H), 7.39–7.32 (m, 2H, Ar'H) 7.29 (dd,  $J = 5.2$ , 3.8, 1H, Ar'H), 7.29 (dd,  $J = 5.0$ , 3.7, Hz, 1H, ThiophenylH), 7.06 (s, 2H, ArH), 4.68 (s, 2H,  $\text{CH}_2\text{OH}$ ).  $^{13}\text{C}$  NMR (100 MHz,  $(\text{CD}_3)_2\text{CO}$ ),  $\delta$  187.5, 173.3, 156.4, 144.4, 142.9, 138.9, 135.4, 135.2, 134.3, 130.2, 129.9, 129.1, 128.6, 126.2, 121.6, 108.9. HRMS:  $m/z$  calculated for  $\text{C}_{18}\text{H}_{15}\text{O}_4\text{S}$ ,  $[\text{M}+\text{H}]^+$  327.0691, found: 327.0677.

#### 4.2.48. (3,5-Dihydroxy-4-pyridin-3-yl-phenyl)-thiophen-2-yl-methanone (45)

Pale yellow solid (9.4 mg, 66%). Analytical UPLC retention time 2.09 min; purity 99.5%.  $^1\text{H}$  NMR, (400 MHz,  $(\text{CD}_3)_2\text{CO}$ ),  $\delta$  8.70 (dd,  $J =$

2.0 Hz, 0.4 Hz, 1H, PyridylH), 8.50 (dd,  $J = 4.7$  Hz, 2.0 Hz, 1H, PyrH), 7.99 (dd,  $J = 5.1$ , 1.0 Hz, 1H, ThiophenylH), 7.88 (dt,  $J = 7.9$ , 1.7 Hz, 1H, PyridylH), 7.83 (dd,  $J = 3.8$ , 1.1 Hz, 1H, ThiophenylH), 7.42 (dd,  $J = 7.9$ , 0.8 Hz, 1H, PyridylH), 7.29 (dd,  $J = 5.0$ , 3.7, Hz, 1H, ThiophenylH), 7.09 (s, 2H, ArH).  $^{13}\text{C}$  NMR (100 MHz,  $(\text{CD}_3)_2\text{CO}$ ),  $\delta$  187.4, 170.9, 156.6, 152.4, 148.6, 144.3, 139.7, 138.9, 135.5, 135.4, 130.7, 129.1, 123.6, 117.9 108.9. HRMS:  $m/z$  calculated for  $\text{C}_{16}\text{H}_{12}\text{NO}_3\text{S}$ ,  $[\text{M}+\text{H}]^+$  298.0538, found: 298.0535.

#### 4.3. Biological reagent and supplies

The HEK-CNG parental, HEK-CNG + CB1 (human), and HEK-CNG + CB2 (human) cell lines, and ACTOne Membrane Potential Dye were purchased from Codex BioSolutions, Inc (Gaithersburg, MD). Tango™ CNR2-bla and CNR1-bla U2OS human cell lines were purchased from Invitrogen (Carlsbad, CA). C8-B4 (ATCC® CRL-2540™) was purchased from ATCC (Manassas, Virginia). Immortalized Human Microglia SV40 was purchased from ABM (Richmond, BC). Puromycin, DMEM, penicillin/streptomycin, gentamicin, PBS, 0.25% Trypsin/EDTA, Hank's Buffer, HEPES, EDTA, Tris base, sucrose,  $\text{MgCl}_2$ , Millipore filter plates and punch kits, EcoLite scintillation cocktail, and Poly-d-lysine coated 96 well plates catalog # 356,461 were purchased from Fisher Scientific (Waltham, MA). G418 was purchased from KSE Scientific (Durham, NC). FBS was purchased from Atlanta Biologicals (Flowery Branch, GA). Ro 20-1724, acetonitrile, DMSO, polyethylene amine, and fatty acid-free BSA were purchased from Sigma Aldrich (St. Louis, MO). Forskolin and CP 55,940 were purchased from Tocris (Bristol, UK). LiveBLazer™-FRET B/G Loading Kit, Solution D, Recovery™ Cell Culture Freezing Medium, FreeStyle™ Expression Medium, McCoy's 5A Medium (modified) (1X), fetal bovine serum (FBS) dialyzed, Non-essential amino acids (NEAA), sodium pyruvate, HEPES (1 M, pH 7.3), 0.05% Trypsin/EDTA, Zeocin™, Hygromycin, Geneticin were purchased from Invitrogen (Carlsbad, CA). Black-wall, clear-bottom, 96-well assay plates #3603 were purchased from Corning (Corning, NY). Tritiated [ $^3\text{H}$ ]-CP 55,940 was purchased from PerkinElmer (Waltham, MA). The 96-well filter plates and punch tips were purchased from Millipore (Billerica, MA). Pierce BCA protein assay kit and Fisherbrand™ 7 mL Borosilicate Glass Scintillation Vial were purchased from Thermofisher (Waltham, MA). Ecolite(+) LC Fluid, MP Biomedicals was purchased from Tocris (Minneapolis, MN). Dojindo Molecular Technologies IncSupplier Diversity Partner Cell Counting Kit-8 (NC9864731) was purchased from Thermofisher (Waltham, MA). Lipopolysaccharide (LPS) from Escherichia coli O111: B4 (L2630) was purchased from Sigma Aldrich (St. Louis, MO). Antibodies against murine CD 16/32 (ab25235), CD 68 (ab213363), CD 204 (ab123946) and CD 206 (ab64693) were purchased from Abcam (Cambridge, UK). The human CD16 antibody was purchased from R&D systems. Meso-Scale Discovery (MSD) high bind plates (L15XB), anti-rat (R32AH-5), and anti-rabbit (R32AB-5) SULFO-TAG antibodies were purchased from Meso-Scale Discovery (Gaithersburg, MD). Prigrow III Medium (TM003) was purchased from ABM (Richmond, BC).

##### 4.3.1. Cell culture

CNR2-bla and CNR1-bla U2OS cell lines were cultured in McCoy's 5A medium with 10% dialyzed FBS, 1% P/S, 0.1 mM NEAA, 25 mM HEPES, 1 mM sodium pyruvate, 200  $\mu\text{g}/\text{ml}$  Zeocin™, 50  $\mu\text{g}/\text{ml}$  Hygromycin, 100  $\mu\text{g}/\text{ml}$  Geneticin. CNR2-bla and CNR1-bla U2OS cells were passaged every 2 to 3 days or when confluence reach 80%. HEK-CNG + CB1 and HEK-CNG + CB2 cells were cultured in DMEM with 10% FBS, 1% P/S, 250  $\mu\text{g}/\text{ml}$  G418, and 5  $\mu\text{g}/\text{mL}$  puromycin. HEK-CNG cells were cultured in DMEM with 10% FBS, 1% P/S, and 250  $\mu\text{g}/\text{ml}$  G418. HEK-CNG + CB1 and HEK CNG + CB2 cells were passaged every 2–3 days or when confluence reached 80%. C8B4 cells were cultured in DMEM with 10% FBS, 1% P/S, and passaged every one or two weeks or when confluence reaches 80%. Immortalized SV40 human microglia were maintained in Prigrow III media with 1% P/S and 10% FBS and were passaged every

2–3 days or when confluence reached 80%. Cell culture flasks were changed every five passages or after two weeks of use.

Unless otherwise stated, all cell culture experiments wherein incubation is stated used humidified incubation chambers maintained at 37 °C and 5%  $\text{CO}_2$ .

##### 4.3.2. Membrane preparations

The membrane preparations were prepared from the functional cell lines HEK-CNG + CB1 or HEK-CNG + CB2 cell lines. Briefly, HEK-CNG + CB1 or HEK-CNG + CB2 cells were plated in 500  $\text{cm}^2$  culture dishes and incubated for two days or when it reached 80 to 90% confluence. Media was removed and cells were washed with 10 mL of ice-cold PBS. Cells were scrapped after the addition of 10 mL of ice-cold PBS with 10 mmol/L EDTA and the cell suspension was centrifuged at 4 °C, 500g for 5 min. The supernatant was discarded, and the pellet homogenized in 10 mL of solution A (50 mM Tris HCL, 320 mM sucrose, 2 mM EDTA, and 5 mM  $\text{MgCl}_2$ ). The cell suspension was centrifuged at 4 °C, 1600g for 10 min. The supernatant was saved, and the cell pellet washed three times in 8 mL of solution A. All supernatants were combined and centrifuged at 4 °C, 50,228g for 3 h. The supernatant was discarded, and the pellet was suspended in 3 mL of solution B (50 mM Tris HCL, 10% sucrose, 2.5 mM EDTA, and 5 mM  $\text{MgCl}_2$ ). Protein concentration was determined using a Pierce BCA protein assay kit and membrane aliquots were stored at –80 °C. Scatchard analysis was carried out on CB1 and CB2 membrane preparations yielding a  $K_d = 1.4$  nmol/L and  $B_{\text{max}} = 1.7$  pmol/mg for CB1 and for CB2 a  $K_d = 2.3 \pm 0.8$  nmol/L with  $B_{\text{max}} 1.25 \pm 0.35$  pmol/mg.

##### 4.3.3. Receptor binding assays

Millipore filter plates were filled with 210  $\mu\text{L}/\text{well}$  of 0.05% (w/v) polyethylene amine in deionized water and incubated for 1 h at room temperature. Plates were washed five times with 250  $\mu\text{L}/\text{well}$  of deionized water then filtered using a vacuum manifold before starting the experiment. After plate coating, 125  $\mu\text{L}$  binding buffer was added to each well, followed by the addition of 5  $\mu\text{L}$  of [ $^3\text{H}$ ]-CP 55,940, 10  $\mu\text{g}$  of membrane protein in binding buffer, and 50  $\mu\text{L}$  of a test compound in binding buffer (final concentration ranging from 1 nmol/L to 10  $\mu\text{mol}/\text{L}$ ). Plates were incubated at 30 °C for 1.5 h, then solutions were removed via vacuum and washed nine times with binding buffer. The plates were vacuumed dry and punch tips were used to eject the filters into 5 mL of Eco-lite scintillation cocktail in 7 mL scintillation vials. Counts per minute (CPM) were measured the next day using PerkinElmer Liquid Scintillation Analyzer Tri-Carb 2810TR, 3-min dwell time. At least six biological replicates were used for data analysis.

##### 4.3.4. Actone cAMP functional assay

The HEK-CNG (parental cell line), HEK-CNG + CB1, and HEK-CNG + CB2 cells were plated in clear poly-d-lysine coated 96-well plates in plating media (DMEM, 10% FBS, 1% P/S) at 50,000 cells/100  $\mu\text{L}$  medium, and plates were incubated for 16–18 h. The next day, 100  $\mu\text{L}$  of ACTOne membrane potential dye was added to each well and the plates were maintained at room temperature for 1 h in the dark. 5X of tested compounds were prepared from  $1 \times 10^{-6}$  to  $1 \times 10^{-9}$  containing 25  $\mu\text{mol}/\text{L}$  Ro 20–1724, and 800 nmol/L forskolin in PBS with 2.5% (v/v) DMSO. Following the addition of the test compounds, plates were read every 5 min using a BioTek (Winooski, VT) plate reader (Ex 540 nm, Em 590 nm) for 1 h. The data at 50 mins were combined and analyzed to calculate the  $\text{EC}_{50}$ . Six to nine biological replicates were used for data analysis. The non-selective agonist CP 55,940 was used as a positive control in each experimental run. An assay was considered acceptable if the  $\text{EC}_{50}$ s for CP 55,940 ranged from 1 to 10 nM and % cAMP suppression was 70 to 95 for both cell lines.

##### 4.3.5. Tango™ -BLA $\beta$ -Arrestins functional assay

CNR2-bla and CNR1-bla U2OS cells were plated in black-wall, clear-bottom, 96 well assay plates in FreeStyle™ Expression Medium at

50,000 cells/100  $\mu$ L well and incubated for 16–18 h. A 10X stock of test compounds was prepared in FreeStyle™ Expression Medium with 0.5% DMSO. The final concentrations of test compounds ranged from  $1 \times 10^{-6}$  to  $10^{-9}$  M and the internal control CP-55,940 at 5  $\mu$ M. Additional controls contained assay medium with 0.5% DMSO was added in the cell-free wells and to unstimulated cell wells. The plates were incubated for 5 h then 20  $\mu$ L of a 6X loading solution, prepared according to the manufacturer's protocol, was added to each well. The plates were incubated at room temperature for an additional 2 h in the dark. Plates were read using Synergy 2 BioTek (Winooski, VT) plate reader (Ex 409/20 nm, Em 460/40 nm, Em 530/30 nm) with fluorescence reading set to a bottom-read mode with optimal gain and 5 reads. CP 55,940 served as a positive control for all runs. An acceptable run was defined by CP 55,940 EC<sub>50</sub> between 30 and 40 nM for CB2 and 1–10 nM for CB1, with % activation range between 80 and 100% for both cell lines. Three to nine biological replicates were used for data analysis.

For the competition (antagonist) assays cells were treated with compound concentrations ranging from  $1 \times 10^{-6}$  to  $10^{-9}$  M and incubated for 30 min. To the cells was then added 10  $\mu$ L of CP 55,940 solution (10X the EC<sub>80</sub>) prepared in an expression assay medium with 0.5% DMSO and allowed to incubate for 5 h. After the incubation interval, 6X loading solution was added to each well and the plates were incubated at room temperature for an additional 2 h protected from light. Plates were read using as before from at least four biological replicates.

#### 4.3.6. Cytotoxicity assays

C8B4 or SV40 cells were plated at 5000–10,000 cells/well (100  $\mu$ L/well) on a 96 well plate and incubated for 24 h. On the second day, the 10% FBS media was replaced with 1% FBS media, and plates were incubated overnight. Compound **40** was added at final concentrations of  $10^{-4}$  to  $10^{-6.5}$  and plates were incubated for an additional 24 h. To the plates was added 10  $\mu$ L of CCK-8 Reagent to each well and the plate was incubated for at least 2 h in the incubator followed by absorbance measurement at 450 nm wavelength using BioTek plate reader.

#### 4.3.7. M1 and M2 murine and human microglia cell surface markers

C8B4 or SV40 cells were plated on 96-well Meso Scale Discovery high bind plate at a density of 20,000 cells in 50  $\mu$ L (10,000 cells in 100  $\mu$ L) per well and incubated overnight. The 10% FBS medium was removed and replaced with 100  $\mu$ L of 1% FBS medium and the plates were incubated for 18–24 h. The following day LPS (final concentration 100 ng/mL) was added to each well and incubated for 1 h (except control wells received 1% FBS media). After 1 h of LPS stimulation, compound **40** was added at 20  $\mu$ M for C8B4 and 35  $\mu$ M for SV40 cells, and plates were incubated for an additional 24 h. The expression of M1 (CD 16/32, CD 16, CD 68) and M2 markers (CD 204, and CD 206) was measured using 30  $\mu$ L per well of antibody prepared in PBS at a concentration of 2  $\mu$ g/mL. After a 2 h incubation on a shaker plate at 130 rpm, wells were washed using 150  $\mu$ L PBS, and 30  $\mu$ L per well of secondary antibody (anti-rat or anti-rabbit) containing Sulfo-tag in PBS was added at a concentration of 2  $\mu$ g/mL. Plates were then incubated for an additional 2 h, washed three times with 150  $\mu$ L per well of PBS, and read in 2X surfactant-free read-buffer using a SECTOR Imager 2400 (Meso Scale Discovery).

#### 4.3.8. Scratch assay

SV40 cells were plated at 50,000 cells/ml on 12 wells collagen I coated plates and incubated overnight. The next day Prigrow III 10% FBS media was replaced with 1% FBS media and the plates were incubated for 18–24 h. Following the equilibration period, a scratch was made using 100  $\mu$ L pipette tip and wells were gently washed twice with 1% FBS Prigrow III media to remove detached and floating cells. Cells were then stimulated with LPS (100 ng/ml) for LPS control and treated wells for 30 mins (control wells received 1% FBS media only). After 30 min LPS stimulation, compound **40** (10  $\mu$ M), prepared in 1% FBS

Prigrow III media containing LPS, was added to the treatment group. Plates were incubated for an additional 24 h. Images from 7 biological replicates were taken at 0 h and 24 h and the number of cells migrated was analyzed using ImageJ.

#### 4.3.9. Microglia morphology – Cytoskeleton staining

SV40 cells were plated on 12 well collagen I coated plates and incubated for 18–24 h. The following day, Prigrow III 10% FBS media was replaced with 1% FBS media, and the plates were incubated for an additional 24 h. The cells were then stimulated with LPS (1  $\mu$ g/ml) or a combination of compound **40** (at 10  $\mu$ M) + LPS (1  $\mu$ g/ml) or left untreated. Plates were incubated for an additional 24 h. Cells were stained using actin cytoskeleton staining kit (FAK100) according to manufacturer protocol. TRITC-conjugated Phalloidin was used to detect F-actin and DAPI was used to stain the nucleus. Ten fields were taken for each group using a BZ-X fluorescence microscope.

#### 4.3.10. Measurement of ROS

SV40 cells were plated at 30,000 cells/ml on 96 well black wall clear bottom collagen I coated plate and incubated for 24 h. The following day the Prigrow III 10% FBS media was replaced with serum-free media and the plates were incubated for 18–24 h. The media was then removed, and dye was added to the cells at 10  $\mu$ M concentration and incubated for 30 min. Plates were washed twice with serum-free media (phenol red-free) and then treated with serum-free media (negative control), LPS (100 ng/ml), or compound **40** (at 10  $\mu$ M) + LPS (100 ng/ml). Reading was taken at 50 min and 24 h. The fluorescence measurement was made using BioTek Synergy 2 (BioTek Instruments, Inc. Winooski, VT) with 485/20 excitation and 528/20 emission filters set to bottom read.

#### 4.3.11. Data analysis

Binding assay  $K_i$  values were determined using Cheng and Prusoff equation.<sup>53</sup> For the ACTOne data, the analysis was done using non-linear regression analysis and fluorescent measurements at 50 mins. The data were normalized using a scaling equation:

$$X' = A + \frac{(X - X_{min})(B - A)}{X_{max} - X_{min}}$$

where A = Blank well-containing dye and cells only, B = Forskolin stimulation, X' = Normalized value, X max = 100%, X = min 0%. The Tango-BLA assay analysis on the fluorescent measurements was carried out by subtracting the background (cell-free wells) from both emission channels (460 nm and 530 nm). Blue/Green Emission Ratio was calculated for each well by dividing the background-subtracted blue emission values by the background-subtracted green emission values.

Background-Subtracted Fluorescence (FI) = FI<sub>Sample</sub> - FI<sub>Cell-free control</sub>

$$\text{Emission Ratio (ER)} = \frac{\text{Coumarin Emission (460 nm)}}{\text{Fluorescein Emission (530 nm)}}$$

#### Funding

This research did not receive any specific grant from funding agencies in the public, commercial, or not-for-profit sectors.

#### Declaration of Competing Interest

The authors declare that they have no known competing financial interests or personal relationships that could have appeared to influence the work reported in this paper.

#### Acknowledgments

This research was supported by Dr. Kennard Brown and the Plough Center for Sterile Drug Delivery Systems, University of Tennessee Health Science Center. The fellowship for S.S.A. was provided by King Saud Bin

Abdul Aziz University for Health Sciences (KSAU-HS) Riyadh, 11426, Saudi Arabia. We thank Dr. Dejian Ma for conducting the high-resolution mass spectrometry and UPLC analysis of the final products.

Current address for Sahar S. Alghamdi

College of Pharmacy, Department of Pharmaceutical Sciences, King Saud bin Abdulaziz University for Health Sciences (KSAU-HS), Riyadh, Saudi Arabia.

King Abdullah International Medical Research Center (KAIMRC), Ministry of National Guard Health Affairs, Riyadh, Saudi Arabia.

## Appendix A. Supplementary material

Supplementary data to this article can be found online at <https://doi.org/10.1016/j.bmc.2021.116035>.

## References

- Neurath MF. Targeting immune cell circuits and trafficking in inflammatory bowel disease. *Nat Immunol*. 2019;20:970–979.
- Coussens LM, Werb Z. Inflammation and cancer. *Nature*. 2002;420:860–867.
- Wyss-Coray T, Mucke L. Inflammation in Neurodegenerative Disease—A Double-Edged Sword. *Neuron*. 2002;35:419–432.
- Sostres C, et al. Adverse effects of non-steroidal anti-inflammatory drugs (NSAIDs, aspirin and coxibs) on upper gastrointestinal tract. *Best Pract Res Clin Gastroenterol*. 2010;24:121–132.
- Oray M, et al. Long-term side effects of glucocorticoids. *Expert Opin Drug Safety*. 2016;15:457–465.
- Li P, Zheng Y, Chen X. Drugs for autoimmune inflammatory diseases: from small molecule compounds to anti-TNF biologics. *Front Pharmacol*. 2017;8:460.
- Monaco C, et al. Anti-TNF therapy: past, present and future. *Int Immunol*. 2015;27:55–62.
- Pardridge WM. Blood-brain barrier delivery. *Drug Discov Today*. 2007;12:54–61.
- Zlokovic BV. The blood-brain barrier in health and chronic neurodegenerative disorders. *Neuron*. 2008;57:178–201.
- Kumar A, Loane DJ. Neuroinflammation after traumatic brain injury: Opportunities for therapeutic intervention. *Brain Behav Immun*. 2012;26:1191–1201.
- Heneka MT, et al. Neuroinflammation in Alzheimer's disease. *Lancet Neurol*. 2015;14(4):388–405.
- Tansey MG, Goldberg MS. Neuroinflammation in Parkinson's disease: Its role in neuronal death and implications for therapeutic intervention. *Neurobiol. Dis*. 2010;37:510–518.
- Aguzzi A, Barres BA, Bennett ML. Microglia: scapegoat, saboteur, or something else? *Science*. 2013;339:156–161.
- Jung YJ, et al. Neuroinflammation as a factor of neurodegenerative disease: thalidomide analogs as treatments. *Front Cell Dev Biol*. 2019;7:313.
- Elewa HF, et al. Minocycline for acute neuroprotection. *Pharmacotherapy*. 2006;26:515–521.
- Lauterbach EC. Repurposing psychiatric medicines to target activated microglia in anxious mild cognitive impairment and early Parkinson's disease. *Am J Neurodegener Dis*. 2016;5:29–51.
- Villapol S. Roles of peroxisome proliferator-activated receptor-gamma on brain and peripheral inflammation. *Cell Mol Neurobiol*. 2018;38:121–132.
- Ashton JC, Glass M. The cannabinoid CB2 receptor as a target for inflammation-dependent neurodegeneration. *Curr Neuropharmacol*. 2007;5:73–80.
- Gómez-Gálvez Y, et al. Potential of the cannabinoid CB(2) receptor as a pharmacological target against inflammation in Parkinson's disease. *Prog Neuropsychopharmacol Biol Psychiatry*. 2016;64:200–208.
- Benito C, et al. Cannabinoid CB2 receptors and fatty acid amide hydrolase are selectively overexpressed in neuritic plaque-associated glia in Alzheimer's disease brains. *J Neurosci*. 2003;23:11136–11141.
- Ramírez SH, et al. Attenuation of HIV-1 replication in macrophages by cannabinoid receptor 2 agonists. *J Leukoc Biol*. 2013;93:801–810.
- Yiangou Y, et al. COX-2, CB2 and P2X7-immunoreactivities are increased in activated microglial cells/macrophages of multiple sclerosis and amyotrophic lateral sclerosis spinal cord. *BMC Neurol*. 2006;6:12.
- Donat CK, et al. Microglial activation in traumatic brain injury. *Front Aging Neurosci*. 2017;9:208.
- Bayewitch M, et al. The peripheral cannabinoid receptor: adenylate cyclase inhibition and G protein coupling. *J FEBS Lett*. 1995;375(1–2):143–147.
- Bouaboula M, et al. Signaling pathway associated with stimulation of CB2 peripheral cannabinoid receptor Involvement of both mitogen-activated protein kinase and induction of Krox-24 expression. *Eur J Biochem*. 1996;237:704–711.
- Rhee M-H, Kim S-K. SR144528 as inverse agonist of CB2 cannabinoid receptor. *J Vet Sci*. 2002;3:179–184.
- Cabral GA, Griffin-Thomas L. Emerging role of the CB2 cannabinoid receptor in immune regulation and therapeutic prospects. *Expert Rev Mol Med*. 2009;11, e3.
- Turcotte C, et al. The CB2 receptor and its role as a regulator of inflammation. *Cell Mol Life Sci*. 2016;73:4449–4470.
- Dhopeshwarkar A, Mackie K. CB2 cannabinoid receptors as a therapeutic target—what does the future hold? *Mol Pharmacol*. 2014;86:430–437.
- Tabrizi MA, et al. Medicinal chemistry, pharmacology, and potential therapeutic benefits of cannabinoid CB2 receptor agonists. *Chem Rev*. 2016;116:519–560.
- Lunn C, et al. Biology and therapeutic potential of cannabinoid CB2 receptor inverse agonists. *Br J Pharmacol*. 2008;153:226–239.
- Lunn CA. Updating the chemistry and biology of cannabinoid CB2 receptor – specific inverse agonists. *Curr Top Med Chem*. 2010;10:768–778.
- Iwamura H, et al. In vitro and in vivo pharmacological characterization of JTE-907, a novel selective ligand for cannabinoid CB2 receptor. *J Pharmacol Exp Ther*. 2001;296:420–425.
- Lunn CA, et al. A novel cannabinoid peripheral cannabinoid receptor-selective inverse agonist blocks leukocyte recruitment in vivo. *J Pharmacol Exp Ther*. 2006;316(2):780–788.
- Rinaldi-Carmona M, et al. SR 144528, the First Potent and Selective Antagonist of the CB2 Cannabinoid Receptor. *J Pharmacol Exp Ther*. 1998;284:644–650.
- Presley C, et al. Preclinical evaluation of SMM-189, a cannabinoid receptor 2-specific inverse agonist. *Pharmacol Res Per*. 2015;3(4):e00159.
- Reiner A, et al. Motor, visual and emotional deficits in mice after closed-head mild traumatic brain injury are alleviated by the novel CB2 inverse agonist SMM-189. *Int J Mol Sci*. 2015;16(1):758–787.
- Bu W, et al. Mild traumatic brain injury produces neuron loss that can be rescued by modulating microglial activation using a CB2 receptor inverse agonist. 2016;10:449.
- Guley NM, et al. Amelioration of visual deficits and visual system pathology after mild TBI with the cannabinoid type-2 receptor inverse agonist SMM-189. *Exp Eye Res*. 2019;182:109–124.
- Liu Y, et al. Abnormalities in dynamic brain activity caused by mild traumatic brain injury are partially rescued by the cannabinoid type-2 receptor inverse agonist SMM-189. *eNeuro*. 2017;18. ENEURO.0387-16.2017.
- Yu Y, et al. Inverse agonism of cannabinoid receptor type 2 confers anti-inflammatory and neuroprotective effects following status epilepticus. *Mol Neurobiol*. 2020;57:2830–2845.
- Presley CS, et al. Synthesis and biological evaluation of (3', 5'-dichloro-2, 6-dihydroxy-biphenyl-4-yl)-aryl/alkyl-methanone selective CB2 inverse agonist. *Biorg Med Chem*. 2015;23(17):5390–5401.
- Presley JD, et al. Selective cannabinoid 2 receptor stimulation reduces tubular epithelial cell damage after renal ischemia-reperfusion injury. *J Pharmacol Exp Ther*. 2018;364:287–299.
- Fillion E, Fishlock D. Total synthesis of (+/-)-taiwaniaquinol B via a domino intramolecular friedel-crafts acylation/carbonyl  $\alpha$ -tert-alkylation reaction. *J Am Chem Soc*. 2005;127:13144–13145.
- Berliner MA, Belecki K. Simple, rapid procedure for the synthesis of chloromethyl methyl ether and other chloro alkyl ethers. *J Org Chem*. 2005;70:9618–9621.
- Krishnamurthy M, Gurley S, Moore II BM. Exploring the substituent effects on a novel series of C10-dimethyl-aryl  $\Delta^8$ -tetrahydrocannabinol analogs. *Bioorg Med Chem*. 2008;16:6489–6500.
- van der Lee MMC, et al. Pharmacological characterization of receptor redistribution and beta-arrestin recruitment assays for the cannabinoid receptor 1. *Biomol. Screen*. 2009;14:811–823.
- Alliot F, et al. A spontaneously immortalized mouse microglial cell line expressing CD4. *Dev Brain Res*. 1996;95:140–143.
- Abd-El-Basset E, Fedoroff S. Effect of bacterial wall lipopolysaccharide (LPS) on morphology, motility, and cytoskeletal organization of microglia in cultures. *J Neurosci Res*. 1995;41:222–237.
- Neubrand VE, et al. Mesenchymal stem cells induce the ramification of microglia via the small RhoGTPases Cdc42 and Rac1. *Glia*. 2014;62:1932–1942.
- Popa-Wagner A, et al. ROS and brain diseases: the good, the bad, and the ugly. *Oxid Med Cell Longev*. 2013;14.
- Ribeiro R, et al. Involvement of ERK1/2, cPLA2 and NF- $\kappa$ B in microglia suppression by cannabinoid receptor agonists and antagonists. *Prostag Oth Lipid M*. 2013;100:1–14.
- Cheng Y, Prusoff W. Relationship between Ki and IC50 of an enzymatic reaction. *Biochem. Pharmacol*. 1973;22:3099–3103.